



Norwegian University of  
Science and Technology

# Experimental and numerical investigations of loads on aquaculture nets

**Jialing Yu**

Marine Technology

Submission date: June 2017

Supervisor: Trygve Kristiansen, IMT

Co-supervisor: Martin Søreide, Aqualine

Norwegian University of Science and Technology  
Department of Marine Technology



## **Preface**

This is the master thesis in the specialization of Marine Hydrodynamics, at the department of Marine Technology, NTNU, Trondheim, Norway. It was carried out during the spring semester of 2017. It was carried out and cooperated under the support of Aqualine. Aqualine has proposed the idea of the project and provided the nets for experimental tests. Prof. Trygve Kristiansen has extended and developed the project and finally determined the title of the project.

Trondheim, 2017-06-11

Jialing Yu

## Acknowledgment

Here I should sincerely thank my supervisor Trygve Kristiansen (professor, NTNU, Trondheim) for his guidance and instruction during the master project and master thesis period. I would also like to give my great appreciation to the guidance of OpenFOAM from Hao Chen (PhD student, DTU, Denmark) and Tufan Arslan (senior engineer, NTNU, Trondheim) and the help from Mael Moreau (master student, NTNU, Trondheim) for the initiation of CFD simulation.

I would also like to thank Trond Innset (Marintek, Trondheim), Torgeir Wahl (Marintek, Trondheim), Terje Rosten (Marintek, Trondheim), Ole Erik Vinje (Marintek, Trondheim) and Markus (Marintek, Trondheim) for their great help as well as the cooperation from Mael Moreau during the experiment period in January and February, 2017.

Last but not least, I acknowledge the contribution and give thanks to Martin Søreide (Aqualine) and Aqualine for their instruction and support of the project.

Jialing Yu

## Summary and Conclusions

This master thesis is to investigate the drag forces on net panels with different twine diameter, material, solidity ratio, and Reynolds number. A series of net panel towing tests has been carried out. Resistance force on the net panel was measured. The nets have been tested in current only condition, wave only condition and current with wave condition with a representative range of current velocity, wave period and wave steepness. Error and uncertainty in the net panel towing test are analyzed in detail. Numerical simulations were implemented. The numerical simulation in this thesis is realized in the framework of the open source computational fluid dynamics toolbox OpenFOAM with version 4.1. The porous media model was proposed to solve the flow characteristics through and around a net panel. A variety of net panels with different solidity ratio from experiments are applied in the validation case. The porous resistance force was obtained from numerical simulation to compare with the drag force in current only condition from experiments. Satisfactory agreement between simulations and experiments was demonstrated.

# Contents

Preface . . . . .	i
Acknowledgment . . . . .	ii
Summary and Conclusions . . . . .	iii
<b>1 Introduction</b>	<b>2</b>
1.1 Background . . . . .	2
1.2 Literature Review . . . . .	3
1.3 Objectives . . . . .	5
1.4 Thesis Structure . . . . .	5
<b>2 Theory</b>	<b>6</b>
2.1 Screen Type Force Model . . . . .	6
2.2 Porous Media Model . . . . .	8
2.2.1 Governing Equation . . . . .	9
2.2.2 Quadratic Drag Resistance Coefficients . . . . .	11
<b>3 Experimental investigation</b>	<b>13</b>
3.1 Experimental Set-up . . . . .	13
3.1.1 Description of Experimental Set-up . . . . .	13
3.1.2 Solidity Estimation . . . . .	16
3.1.3 Empty Frame Test . . . . .	17
3.2 Results and Discussion . . . . .	20
3.2.1 Current Only . . . . .	20
3.2.2 Wave Only . . . . .	25

<i>CONTENTS</i>	1
3.2.3 Current and Wave . . . . .	29
3.3 Error and Uncertainty . . . . .	32
3.4 Comments . . . . .	35
<b>4 Numerical Investigation</b>	<b>37</b>
4.1 Numerical Set-up . . . . .	37
4.1.1 Description of Model Set-up . . . . .	37
4.1.2 Convergence Test . . . . .	41
4.2 Results and Discussion . . . . .	43
4.3 Comments . . . . .	53
<b>5 Conclusion</b>	<b>55</b>
5.1 Further Work . . . . .	56
<b>A Sn results by GIMP</b>	<b>57</b>
<b>B Power Spectral Density</b>	<b>60</b>
<b>C Time Series</b>	<b>66</b>
C.1 Current Only . . . . .	66
C.2 Wave Only . . . . .	69
C.3 Current with Wave . . . . .	71
<b>Bibliography</b>	<b>74</b>

# Chapter 1

## Introduction

### 1.1 Background

Demand is increasing in food with the increasing of world population. The marine food has only been consumed for a very small percent comparing to the land food, so the exploitation and production of marine food are unavoidable. The trend, nowadays, is to move the fish farms to more exposed areas where fish farms will suffer larger waves and stronger currents. Moreover, the dimensions of the fish farms are expected to increase. In this case, the hydrodynamic forces on fish farms are to be carefully predicted not only for the safety and financial consideration but also for fish welfare. It is known that the water motion and water quality are critical factors for the kindness to fish. Rational analytical and numerical methods are necessary for design purposes since the traditional methods can no longer applicable for the urge nowadays.

For a traditional type of fish cage, which mainly consists of floater and net, loads on the net contribute the most part. In particular, drag force is the dominating contribution of the hydrodynamic force. Question is, how well the loads are predicted. In the past, loads are estimated using models without considering Reynolds number effects, i.e. Morison type model. The force on each twine is summed up to get the total force on the net, and it does not take the interaction between twines into account. Morison force model is proved to be under-estimated for loads on aquaculture nets. However, in experiments, Reynolds number is much smaller than that in

full scales while Reynolds effects are truly important when predicting the hydrodynamic loads. Thus, Kristiansen and Faltisen in 2012, proposed a screen type model which accounts for the Reynolds number effect when predicting the drag force on a net panel. The fish cage is approximated by a system of trusses. The trusses in turn define a number of flat panels (screens). A modified flow velocity including the local speed-up was proposed to account for the flow interaction between the twines. The Reynolds number is taken into account by explicitly being included in the expression of the drag coefficient of a circular cylinder. In addition, numerical study is supplemented to make comparisons. Numerical simulation with the porous media model has been successfully applied to model the current and wave interaction with traditional permeable coastal structures and recently, it has been applied to simulate the flow through and around fishing net structures. Porous media model in numerical simulation is a rather general topic that have been used widely in petroleum engineering, environmental engineering etc, and nowadays it has been more and more popularized to the marine industry.

## 1.2 Literature Review

Experimental and numerical methods have been developed to calculate the drag forces on aquaculture nets since long ago. Løland proposed a screen model, of which drag and lift coefficient are functions of solidity ratio  $S_n$  within a limited range (0.13-0.317) and angle  $\theta$ . The formulas of drag and lift coefficients are determined by curve fitting experimental data by [Rudi et al. \(1988\)](#). [Zhan et al. \(2006\)](#) provided new formulas based on experimental data for planar nets and it was verified also applicable for cylindrical nets. In their paper, analytical formulae for the total normal drag on planar and cylindrical nets are also derived with either square or square diamond mesh patterns. [Lader and Fredheim \(2006\)](#) applied Løland's formula to investigate the dynamic behavior of a net in waves and current by using a numerical model. Impact of five parameters are investigated, including floater movement, wave period, wave height, current velocity, net solidity and bottom weight. [Kristiansen and Faltinsen \(2012\)](#) has proposed a screen type of force model, which assumed the net can be divided into a number of flat net panels or screens. This is a generalization of the screen model proposed by Løland. Differ from the traditional Morison

type model, the screen model proved to be more accurate because it includes the local speed-up of the flow between twines. Reynolds number effects are also included in their hydrodynamic force model. [Kristiansen and Faltinsen \(2015\)](#) further developed their model (2012), and accounted for the regular wave loads. They applied a simplified system which includes the main components of the aquaculture plant: net cage, floater, sinker weights and moorings. Mooring loads are tested under different variables and the relative importance and phasing between inertia and viscous loads were discussed.

[Blevins \(1984\)](#) defined the porous medium as a substance which supports an inter-connecting network of passages that permit fluid flow. [Patursson et al. \(2010\)](#) applied the porous media model to simulate the steady flow through a single net panel, multiplied net panels and gravity cages. The results were verified by experiment measurements and it turned out a good agreement. [Zhao et al. \(2013\)](#) also simulated the flow field around fishing plant nets in current. The unknown porous coefficients are determined from the hydrodynamic forces on the net and from the flow velocities and attack angles using the least squares methods. Turbulent model was applied in this paper. Results showed a good agreement with the experimental data. [Bi et al. \(2014\)](#) accounted for the fluid-structure interaction effect by adding a lumped mass structural model onto the porous media model. The deformation of a net cage can be calculated using the lumped-mass mechanical model and the flow field around a fishing net can be simulated using the porous media fluid model. The comparisons demonstrate that both the configuration of the net chamber and the flow-velocity results are in accordance with those of the corresponding physical model tests. [Zhao et al. \(2014\)](#) extended the application of porous media model into wave interaction with net structures. The volume of fluid (VOF) method is used to track the wave surface. The accuracy of the numerical wave flume is verified through comparison of numerical and theoretical results. [Jensen et al. \(2014\)](#) introduced new calibration cases to the calibration procedure of the resistance coefficients. Simple two and three dimensional uniform caisson structures and breakwater layouts were investigated. The model was implemented in the open source CFD library OpenFOAM and has been made publicly available as part of the wave generation framework waves2Foam. [Chen and Christensen \(2016\)](#) proposed a new approach to calculate the porous resistance coefficients based on the transformation of Morison

type load model. The transformation follows the principle that the total forces acting on a net panel from Morison type load model should be equal to the forces obtained from the porous media model. Two coefficients are added to accounts the effects from all directions. The overall agreement between the numerical and experimental results turned to be fair.

### 1.3 Objectives

The purpose of this thesis is to investigate the drag forces of net panels with different size, material, solidity ratio and Reynolds number. This is realized by both experimental tests and numerical simulations supported by theoretical estimates. The experimental tests are carried out at Lilletanken with the collaboration of Marintek. The present study is based on the analytical model (screen type force model) proposed by [Kristiansen and Faltinsen \(2012\)](#). The numerical simulation is realized using state-of-the-art CFD tools, OpenFOAM ([Greenshields \(2015\)](#)). The numerical model applied in present study is the porous media model. The results both from experimental tests and numerical simulations will be obtained to make comparisons with each other and used to check the validation of the theoretical prediction.

### 1.4 Thesis Structure

The thesis is organized as follows: First, an introduction of the topic will be presented; literature review is also included. Then, the hydrodynamic force model together with the porous media model will be introduced. Next the experimental and numerical investigation will be described respectively, and results and uncertainties are discussed. Finally, conclusion and further work will be presented at the end of the report.

# Chapter 2

## Theory

### 2.1 Screen Type Force Model

The hydrodynamic force model applied in this thesis is the screen type force model proposed by Kristiansen and Faltisen. The fish cage is approximated by a system of trusses and the trusses in turn define a number of flat panels (screens), see figure 2.1. A modified flow velocity including the local speed-up was proposed to account for the flow interaction between the twines. The Reynolds number is taken into account by explicitly being included in the expression of the drag coefficient of a circular cylinder ( $C_D^{circ.cly}$ ). The detailed derivation of the force on screen type model is explained in Kristiansen and Faltinsen (2012). In this thesis, only the final results are presented.

The hydrodynamic force is defined by:

$$F_N = \frac{1}{2} \rho C_N(\theta) A U_{rel}^2 \quad (2.1)$$

where  $\rho$  is the water density, A as the net panel area, and  $U_{rel}$  is the absolute value of the incoming flow velocity. The subscript N indicates the normal direction. If the plane of net panel is perpendicular to the incoming flow direction, one gets the drag force, which means  $F_D = \frac{1}{2} \rho C_N(0) A U_{rel}^2$ . A description of flow and force direction can be found in figure 2.2. The

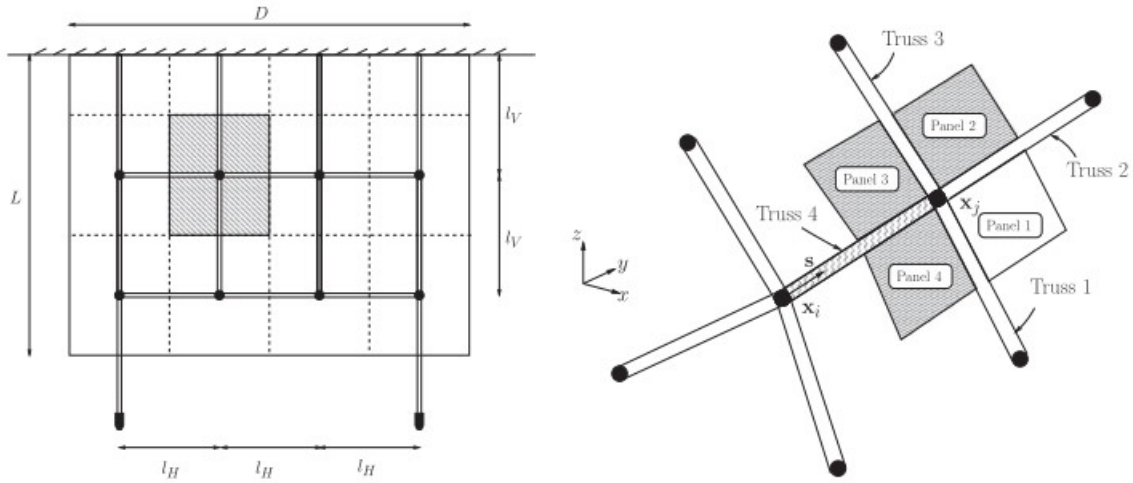


Figure 2.1: Screen model. Left: division of a planar net with dimensions  $L \times D$  into an equivalent truss model.  $l_V$  and  $l_H$  are the lengths of the vertical and horizontal trusses, respectively. Right: net panels represented by shaded areas of arbitrary quadrilateral shape. (Kristiansen and Faltinsen (2012))

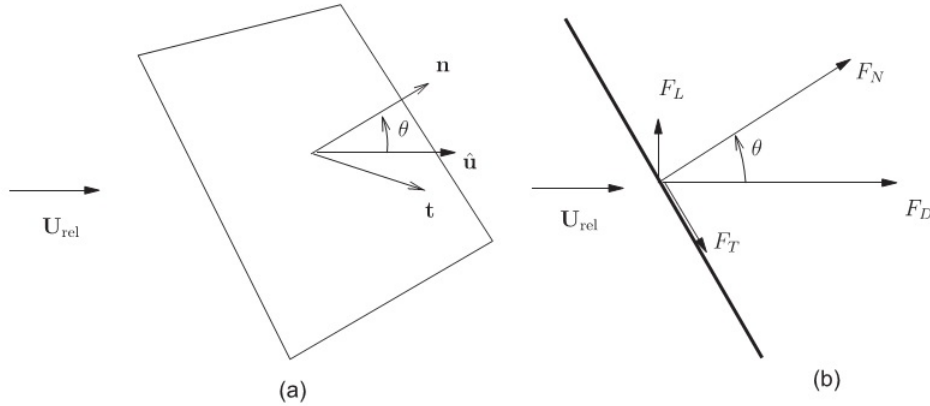


Figure 2.2: Left: unit vectors; the normal unit vector  $\mathbf{n}$  is perpendicular to the panel; the unit tangential vector  $\mathbf{t}$  is in the plane of the panel; the ambient current unit vector  $\hat{\mathbf{u}}$  is in the direction of the local (relative) inflow;  $\theta$  is between the normal and inflow directions. Right: two dimensional force case; drag  $F_D$ , lift  $F_L$ , normal component  $F_N$  and tangential component  $F_T$ . (Kristiansen and Faltinsen (2012))

normalized force coefficient  $C_N(\theta)$  in eq.2.1 is defined as:

$$C_N(\theta) = \frac{C_D^{circ.cly} S_n (1 - 2S_n)}{2(1 - S_n)^2} \cos^2 \theta, \quad 0 \leq \theta \leq \frac{\pi}{4} \quad (2.2)$$

where  $\theta$  is the angle between the normal and inflow direction,  $S_n$  is the solidity ratio, and  $C_D^{circ.cly}$  is the drag coefficient of a circular cylinder. This is valid within range of angle from 0 to  $\frac{\pi}{4}$ . According to Kristiansen and Faltisen, the drag coefficient of a circular cylinder they applied is a 7<sup>th</sup> order polynomial function of the Reynolds number, obtained by Goldstein (1938) from experimental data for Re number range from  $10^{3/2} \leq Re \leq 10^4$ , and it can be expressed as:

$$\begin{aligned} C_D^{circ.cly} = & -78.46675 + 254.73873(\log_{10} Re) - 327.8864(\log_{10} Re)^2 + 223.64577(\log_{10} Re)^3 \\ & - 87.92234(\log_{10} Re)^4 + 20.00769(\log_{10} Re)^5 - 2.44894(\log_{10} Re)^6 \\ & + 0.12479(\log_{10} Re)^7 \end{aligned} \quad (2.3)$$

in which the Reynolds number is:

$$Re = \frac{d_w U_{rel}}{\nu(1 - S_n)} \quad (2.4)$$

where  $\nu$  is the kinematic viscosity of water and  $d_w$  is the twine diameter. These formula can be applied for angle within 0 and  $\frac{\pi}{4}$ .

The procedure to calculate drag coefficient ( $C_D$ ) on a net panel is:

- Calculate the Reynolds number using eq.2.4.
- Calculate  $C_D^{circ.cly}$  with the Reynolds number got from above.
- $C_D = C_N(0)$  gives the drag coefficient with eq.2.2 and  $\theta=0$ .

One can find more information in Kristiansen and Faltinsen (2012).

## 2.2 Porous Media Model

Porous media model in numerical simulation is a rather general topic that have been used widely in petroleum engineering, environmental engineering etc, and nowadays it has been

more and more popularized to the marine industry. It was proposed to solve the flow characteristics through and around aquaculture nets. The basic principle behind is to measure the pressure drop of flow before and behind the porous media and the integral of the pressure drop thus gives the hydrodynamic force on the porous media.

### 2.2.1 Governing Equation

The porous media model was solved in both single phase flow and two phase flow. The solvers was based on the Volume Averaged Reynolds Averaged Navier-Stokes (VARANS) equations, proposed by Jensen et al(2014). The governing equations are given as:

$$\frac{\partial \langle u_i \rangle}{\partial x_i} = 0 \quad (2.5)$$

$$(1 + C_m) \frac{\partial}{\partial t} \frac{\rho \langle \bar{u}_i \rangle}{n} + \frac{1}{n} \frac{\partial}{\partial x_j} \frac{\rho \langle \bar{u}_i \rangle \langle \bar{u}_j \rangle}{n} = - \frac{\partial \langle \bar{p}^f \rangle}{\partial x_i} - g_j x_j \frac{\partial \rho}{\partial x_i} + \frac{1}{n} \frac{\partial}{\partial x_j} \mu \left( \frac{\partial \langle \bar{u}_i \rangle}{\partial x_j} + \frac{\partial \langle \bar{u}_j \rangle}{\partial x_i} \right) - \frac{1}{n} \frac{\partial}{\partial x_j} \rho \langle \overline{u_i' u_j'} \rangle + S_i \quad (2.6)$$

Equation 2.5 is the continuity equation, where  $\langle u_i \rangle$  is the volume averaged ensemble averaged velocity over the total control volume. Equation 2.6 is the momentum equation for porous media. The equation is extended from the Reynolds averaged Navier-Stokes equation, in which  $C_m$  is the added mass coefficient, and it can be expressed as:

$$C_m = \gamma_p \frac{1 - n}{n} \quad (2.7)$$

where  $\gamma_p = 0.34$  is a dimensionless empirical coefficient.

$S_i$  is the porous drag resistance and can be described by the equation proposed by D'arcy (1856) and Forchheimer (1901) in the case of simple homogeneous porous media:

$$S_i = -D_{ij} \mu \langle \bar{u}_j \rangle - \frac{1}{2} \rho C_{ij} \langle \bar{u}_{mag} \rangle \langle \bar{u}_j \rangle \quad (2.8)$$

where  $\langle \bar{u}_{mag} \rangle$  is the magnitude of the fluid velocity and  $D_{ij}$  and  $C_{ij}$  are prescribed material matrices consisting of the porous media resistance coefficients in local  $x_1$ ,  $x_2$  and  $x_3$ -direction. The  $D_{ij}$  and  $C_{ij}$  matrices are defined as:

$$D_{ij} = \begin{bmatrix} D_{11} & 0 & 0 \\ 0 & D_{22} & 0 \\ 0 & 0 & D_{33} \end{bmatrix} \quad (2.9)$$

and

$$C_{ij} = \begin{bmatrix} C_{11} & 0 & 0 \\ 0 & C_{22} & 0 \\ 0 & 0 & C_{33} \end{bmatrix} \quad (2.10)$$

The local axes are the principal axes of the porous media. The first term in Eq. 2.8 states a linear relation between resistance and velocity. The second term considers a non-linear relation. The relative importance of these two terms is dependent on the flow regime, which is based on pore Reynolds number:

$$Re = \frac{u^* d}{\nu} \quad (2.11)$$

where  $\langle \bar{u} \rangle$  is the local velocity at the pore. Usually the Reynolds number of flow through fishing nets is from  $10^2$  to  $10^3$ , within the fully turbulent flow regime, according to the categorization of flow regime defined by Burcharth and Andersen (1995). For this reason, the linear term, which mainly comes from inertia can be negligible, meaning that  $D = 0$ . Only quadratic term is left and the porous drag resistance becomes:

$$S_i = -\frac{1}{2} \rho C_{ij} \langle \bar{u}_{mag} \rangle \langle \bar{u}_j \rangle \quad (2.12)$$

Integrate over the instantaneous wet volume of the porous media, one gets the instantaneous resistance force:

$$Q_i = \frac{1}{2} \rho \int_V C_{ij} \langle \bar{u}_{mag} \rangle \langle \bar{u}_j \rangle dV \quad (2.13)$$

where  $V$  is the instantaneous wet volume of the porous media zone. In this problem, the quadratic coefficient matrix  $C$  is constant (it may vary in some cases, e.g. simulation of flow through cir-

cular gravity cages).

## 2.2.2 Quadratic Drag Resistance Coefficients

As has been discussed before, the linear drag resistance coefficient is zero in this problem. Thus the key point to model the porous media in OpenFOAM is to decide the quadratic drag resistance coefficient. The quadratic resistance coefficient can be derived directly from experimental force or from a rational force model. The basic principle behind is to let the force on porous media be equal to the force from experiment or force model. One should apply a laminar model if the porous resistance coefficient is derived from experimental force since it has already included the turbulent contribution. One should also apply a laminar model if the force model has already taken the turbulence effect into account. In this thesis, both experimental force and force model are applied to derive the numerical force coefficients. Comparison and discussion will be given in chapter 4.

Two load models are mentioned in this thesis: Morison force model and screen type force model. The procedure to calculate the quadratic drag resistance coefficient for Morison force model exactly follows that in [Chen and Christensen \(2016\)](#), in which they defined two coefficients to include the interaction of flow from other directions. The readers can find more details in their paper. Only the final expressions for coefficients are presented here:

$$C_1 = \frac{1}{V} a C_{d,twine} (S_1 + S_2) \quad (2.14)$$

$$C_2 = \frac{1}{V} b C_{d,twine} S_2 \quad (2.15)$$

$$C_3 = \frac{1}{V} b C_{d,twine} S_1 \quad (2.16)$$

where  $S_1$  is the total projected area for in-plane twines and  $S_2$  is that for out-of-plane twines;  $V$  is the instantaneous volume of the porous media zone;  $a$  and  $b$  are interaction coefficients accounting for the shading effect and local speed-up of the flow in-between twines.  $a$  and  $b$

are related to the solidity ratio and their expressions are determined from polynomial fitting of experimental data in [Rudi et al. \(1988\)](#). The final expressions for a and b are given as:

$$a = \begin{cases} 2.348S_n + 1 & 0 < S_n \leq 0.13 \\ 1.3128S_n + 1.1346 & 0.13 < S_n \leq 0.243 \\ 5.3094S_n + 0.1634 & 0.243 < S_n \leq 0.317 \end{cases} \quad (2.17)$$

$$b = \begin{cases} 0.9241 & 0 < S_n \leq 0.13 \\ -0.6310S_n + 1.0061 & 0.13 < S_n \leq 0.243 \\ 8.7581S_n - 1.2754 & 0.243 < S_n \leq 0.317 \end{cases} \quad (2.18)$$

The screen type force model has an expression as defined in equation 2.1, which with  $\theta=0$  is the drag force in direction normal to horizontal inflow direction. The expression has already included the interaction effects from other 2 directions. Thus, when applying screen type force model to derive the quadratic drag resistance coefficient, only coefficient in  $x_1$  direction has the non-zero value (coefficient in  $x_2$  and  $x_3$  direction are set to be zero, namely  $C_{22}=0$  and  $C_{33}=0$ ). Based on this, one has a relation between screen type drag force and porous force:

$$\frac{1}{2}\rho C_N(0)AU_{rel}^2 = \frac{1}{2}\rho \int_V C_{11} \langle \bar{u}_{mag} \rangle \langle \bar{u}_1 \rangle dV \quad (2.19)$$

Here the unknown volume averaged ensemble averaged velocity  $\langle \bar{u} \rangle$  is assumed to be equal to the undisturbed velocity (It is also the assumption in [Chen and Christensen \(2016\)](#)) since the fishing net usually has a very high porosity and the twine diameter is very small, of millimeter magnitude, and thus velocity reduction is small. Now one gets an expression for  $C_{11}$  as:

$$C_{11} = \frac{1}{V} C_N(0)A \quad (2.20)$$

where A is the submerged area of net panel from experiments and V is the wet volume of porous media zone in CFD simulation.

# Chapter 3

## Experimental Investigation

### 3.1 Experimental Set-up

#### 3.1.1 Description of Experimental Set-up

The experimental tests were carried out at Lilletanken, NTNU in January and February 2017, with the collaboration of Marintek. The towing tank has a length of 25 m, 2.8 m width and 1 m depth. Nets with different material properties were tested. They were fixed with strips to a steel frame and towed by the carriage with a representative range of towing speeds. The nets have two types, knotless nylon nets and HDPE (High-density polyethylene) nets with knot connection. The nets have different twine diameters and solidity ratios. Tests are carried out in three situations: current only, wave only and current and wave. The results are all presented in model scale. Froude scaling 1:6 is assumed.

The steel frames were constructed and mounted onto the carriage as shown in figure 3.1. The red steel is part of the carriage system. The silver steel frame was fixed onto the carriage at the top middle side, with two sensors installed measuring the forces. Six wave gauges were fixed at different locations in front of or behind the net to measure the surface elevation. A 2D sketch for the net panel is presented in figure 3.4, drawn by Trond Innset (Marintek). The configuration of the frame bar is a circle with a wedge profile behind, which is to reduce the hydrodynamic interaction on nets from the frame (see figure 3.3 for a cross section sight of the frame bar). The

net was fixed onto the frame with plastic strips (see figure 3.2). The strips go across the net twines and connect the net and the frame and were tied at the outer side of the frame.



Figure 3.1: Experimental set-up. The red steel frame is part of the carriage system. The silver steel frame was fixed onto the carriage at the top middle side, with two sensors installed measuring the forces. Six wave gauges were fixed at different locations in front of or behind the net to measure the surface elevation.



Figure 3.2: Strips layout. The net was stretched by the plastic strips and the strips went through the holes on the frame and were tied at the outer side of the frame.

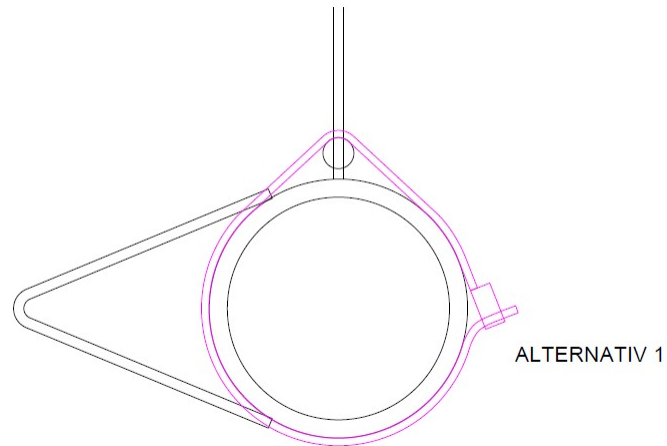


Figure 3.3: Cross section of the frame bar (Figure from Trond Innset, Marintek). The configuration of the frame bar is a circle with a wedge profile behind. The pink part is the sketch of the strip. It goes across the net twines and connects the net and the frame. The rest black part is the net.

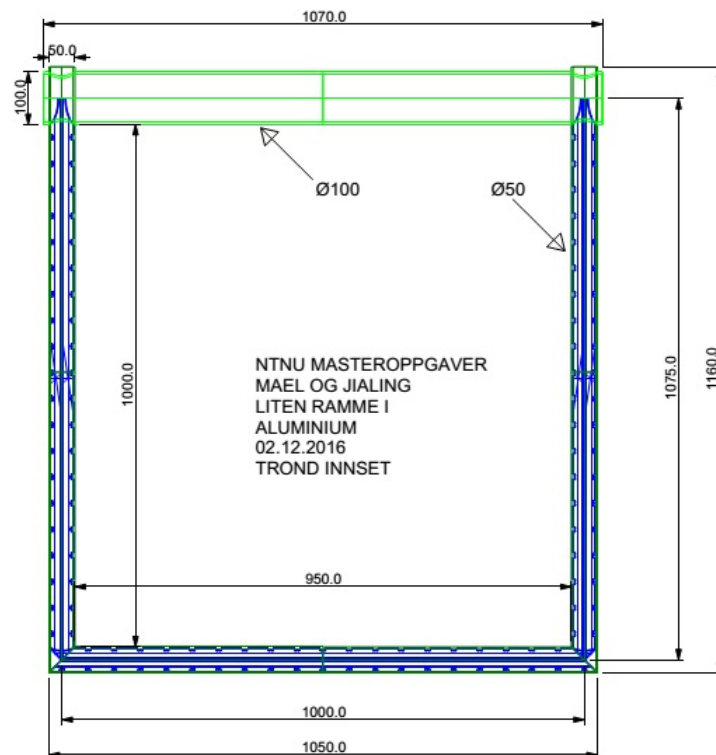


Figure 3.4: 2D net panel overview, drawn by Trond Innset, Marintek. Unit: mm.

### 3.1.2 Solidity Estimation

A traditional approach to estimate the solidity ratio is to measure the twine diameter  $d_w$  and the half mask length  $l$  of the nets, and then the solidity ratio is given by  $S_n = 2d_w/l$ . It may be inaccurate especially when the HDPE net has knots between twines. Moreover, the twine diameter and half mask length labelled on the tag on each net largely deviate from the values measured by vernier caliper in the laboratory.

Another approach to estimate the solidity ratio for each net was using the image analysis technique, called GIMP. The basic principle is to take photos of the net and analyze the colour components of the photos with the Matlab script written by Trygve Kristiansen. In most cases, the photos are in black and white colour (white net with a black background or black net with a white background) and the program will calculate the percentage of the black component. For the nets which have colour other than black and white, an image processing software was applied to transfer the photo into black and white. Figure 3.5 show some examples of the estimation results (More results can be found in Appendix A). From the figures one may find that the light and shadow of the picture will effect the results, and lead to inaccuracy. Moreover, for photos not in black and white, the image processing software will not change the colour into pure black and white and could also affect the results. The difference between the solidity ratios estimated by two techniques for 6 tested nets are shown in table 3.20. From table we can easily find that for HDPE nets with knots, the estimation from two methods are significantly different whereas for knotless nylon net, the results show a relatively better agreement. In this thesis, it was decided to apply the results from GIMP.

Table 3.1: Solidity estimation results from two techniques

Net no.	Type	$d_w$ (mm)	$l$ (mm)	$S_n = 2d_w/l$	$S_n$ by GIMP
1	Nylon	2.4	22.5	0.213	0.217
2	Nylon	2.4	29	0.166	0.164
3	Nylon	2.4	23.9	0.201	0.231
4	HDPE	2.2	25	0.176	0.270
5	HDPE	3.1	75	0.083	0.079
6	HDPE	1.9	18	0.211	0.253

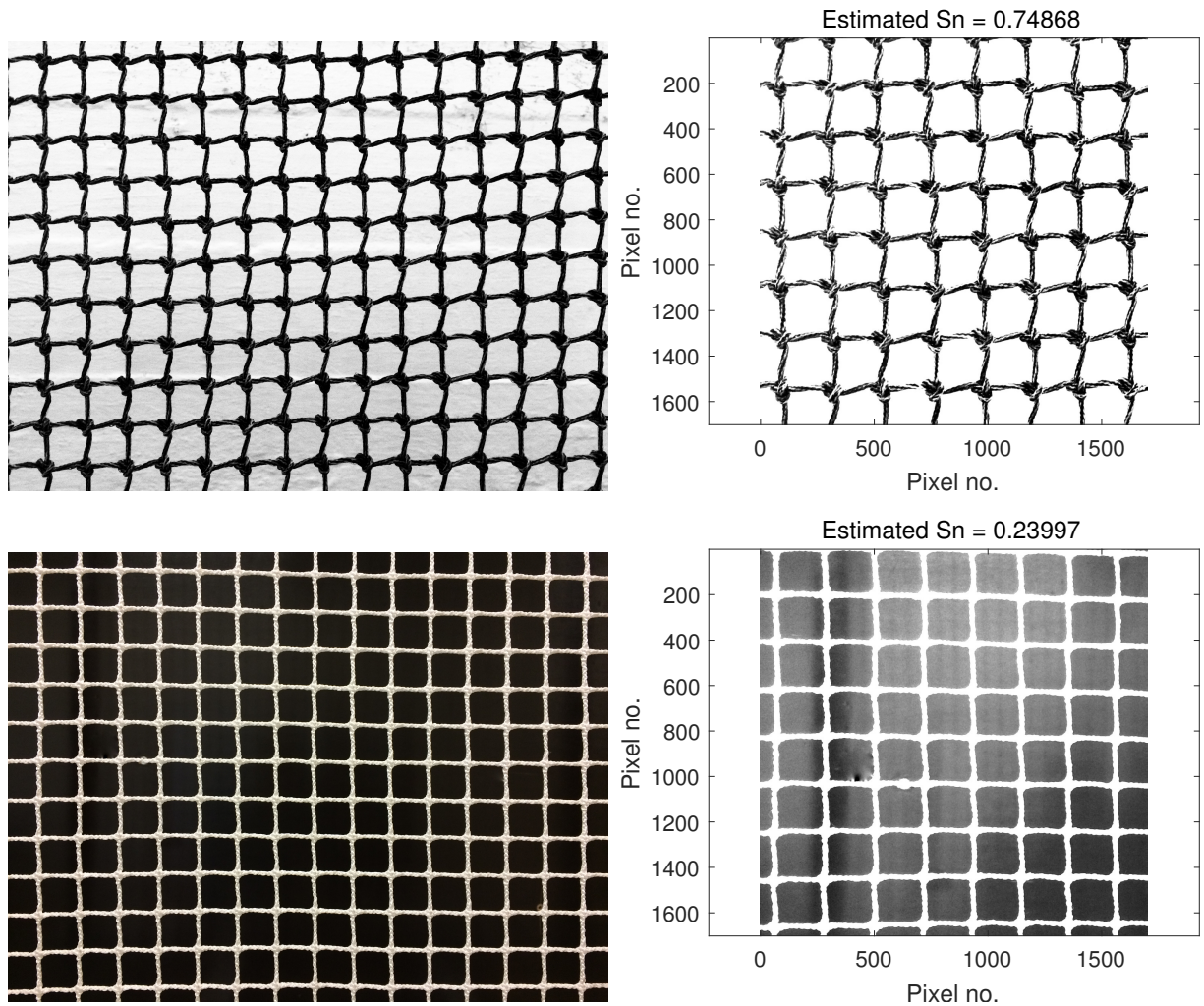


Figure 3.5: Examples of solidity ratio estimation results by GIMP (left side: the original photos; right side: the processed photos marked with the result of estimated solidity ratio)

### 3.1.3 Empty Frame Test

The frame was tested in three conditions: current only condition, wave only condition and current with wave condition, and resistance forces were measured in each condition correspondingly. The frame effect is later subtracted from the total force acting on the frame and the net.

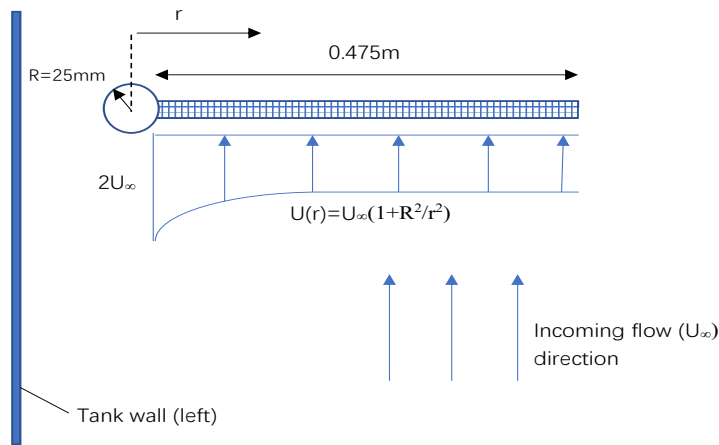
Even though the empty frame force is subtracted from the total force on net panel in experiments, the result is still much higher than the theoretical prediction (see results and detailed discussion in next section). The reason for it is that there are also non-linear effects from frame,

one of which is that the existence of the frame changes the original flow field and causes local speed-up near the frame. The effect should then be added onto the original velocity profile so that one gets a modified flow velocity profile just in front of the net panel.

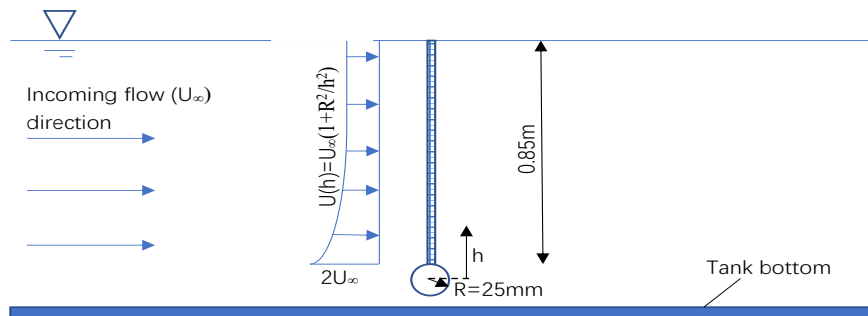
Here one assumes that the cross-section of the frame is circular (in practice it is a circle combined with a wedge profile behind, referring to figure 3.3) and assumes that potential theory is valid. Thus, a modified profile can be obtained. According to the potential theory, the flow around circular cylinder has the velocity tangential to the surface as:

$$u_{\theta} = U_{\infty} \left(1 + \frac{R^2}{r^2}\right) \cos \theta \quad (3.1)$$

where  $U_{\infty}$  is the incoming flow velocity,  $R$  as the radius of circular cylinder,  $r$  as the distance from the center of the circle, and  $\theta$  is the angle between the tangential direction of the stream and the incoming flow direction. At  $\theta = 0$ , regarded as the attached point of the net, the local velocity thus has a maximum of  $2U_{\infty}$  and along the net direction, it decreases asymptotically to incoming flow velocity. The sketch of the modified flow velocity profile from both top view and side view are presented in figure 3.6. The circle is the cross-section of the frame, and the shadow area is the cross-section of net panel. The velocity profile is symmetrical along the net from top view, so only half of the structure and velocity profile are presented in figure 3.6 (a).



(a) Sketch of the modified flow velocity profile (top view). Only half of the net and frame is presented due to symmetry.



(b) Sketch of the modified flow velocity profile (side view)

Figure 3.6: Sketch of the velocity profile after including the local speed-up around the frame. The circle is the cross-section of the frame, and the shadow area is the cross-section of net panel. (a) Top view. (b) Side view.

## 3.2 Results and Discussion

### 3.2.1 Current Only

In current condition, the nets were towed in calm water, of which purpose is to model the net in incoming flow condition. The towing speed was in a range from 0.1m/s to 1.5m/s with a 0.1m/s step. 3 nylon and 3 HDPE nets were tested. Empty frame force is then subtracted from the total force to get the drag force on net. Figure 3.7 shows the total time series of 15 tests on a nylon net with solidity ratio  $S_n = 0.217$ . The trend is, the force grows quadratically with the towing speed; as the towing speed increases, the steady velocity period will get shorter, resulting in a shorter steady force period. Drag forces over velocity and the correspondingly drag coefficients over Reynolds number are illustrated in figure 3.8. Dots with different shapes are the experimental results and the curves are theoretical prediction with the screen type force model.

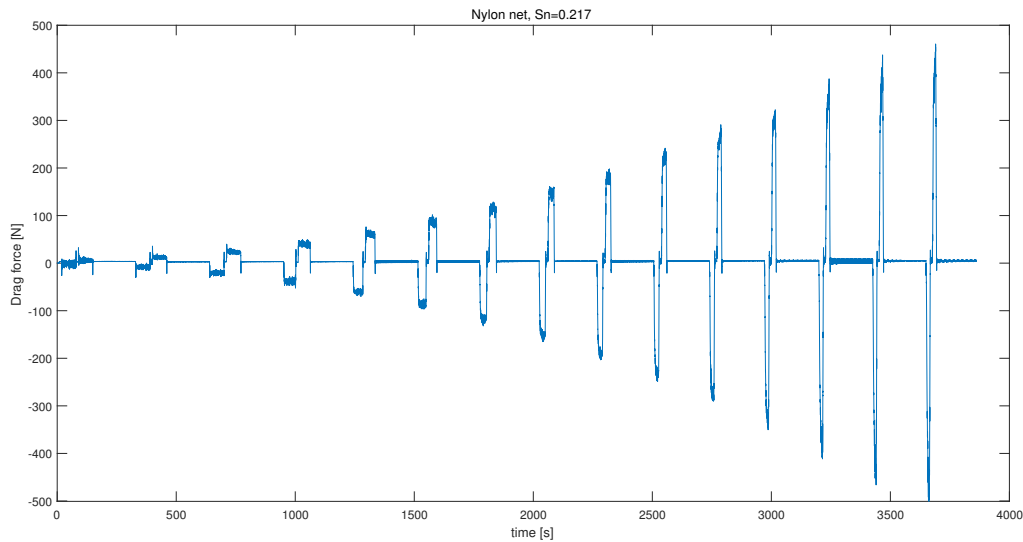


Figure 3.7: Time series of drag force on nylon net with  $S_n=0.217$

The drag forces are plotted over mean incoming flow velocity. For the drag forces, the experimental results are to a certain extent higher than the theoretical ones (Here uniform incoming flow velocity was applied in the calculation). The forces increase quadratically with incoming flow velocity as predicted in the theory, and all experimental data follows the trend. In addition,

under the same speed, the drag force increases with the solidity ratio. One may find one exception for experimental data of HDPE nets with  $S_n=0.253$  and  $S_n=0.27$  (the recorded data is so close to each other and  $S_n=0.27$  gives smaller force). This is explained as a measurement error during the test.

Normalized drag coefficients was plotted over Reynolds numbers. The normalized drag coefficients are higher than the theoretical ones as well. They are initially higher at lower Re number and decrease as the Re number getting bigger. There are some uncertainties when measuring the towing forces and speed during the test, which leads to some abnormal drag coefficient points.

The higher result in experiments is mainly on one side, due to the reality that there are flow through and around the frame, which causes local speed-up around the frame and thus increases the hydrodynamic forces (this has been already mentioned in last section), on other side, due to the interaction between the flow around the twines and thus lead to turbulence behind the twines (The turbulent phenomenon is more obvious for nets with knots).

Once the local speed-up from the frame is included, the modified drag force and drag coefficient can be calculated. Figure 3.9 and Figure 3.10 present the results after using the modified velocity profile. In figure 3.9, the asterisks are experimental data; dash lines are theoretical predictions without modification; solid lines are predictions with modification. The theoretical results after modification show better agreement with the experimental data now. For nylon net, the agreement is better than the result for HDPE net. One supposes that the remain deviation comes from the knots on HDPE nets. The knots among twines disturb the original local flow field and add to more turbulence. Kristiansen proposed a possible solution for accounting for the knot effects. It is to calculate the drag force on net panels separately and then add them together. The expression could be:

$$F_D = F_D^{cir.cyl} + F_D^{knot} \quad (3.2)$$

where  $F_D^{cir.cyl}$  is an equation of the drag coefficient on a circular cylinder with a parameter  $\gamma$  and  $F_D^{knot}$  is an equation of the drag coefficient on a sphere with a parameter  $1 - \gamma$ .  $\gamma$  represents the

percentage of twine area of a net panel and  $1 - \gamma$  is the percentage of knot area of the net panel. Study on the feasibility of this expression can be carried out in the future.

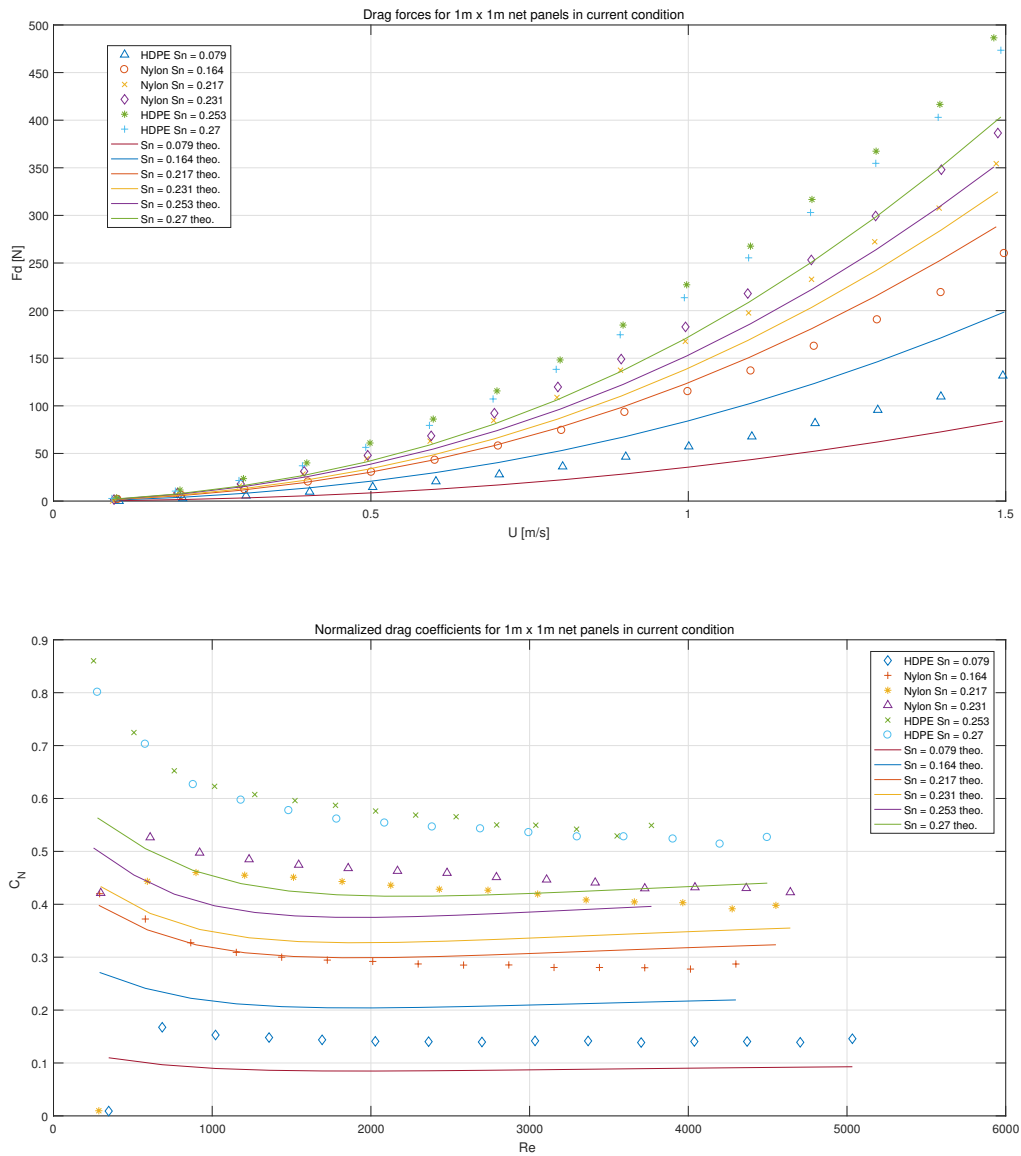


Figure 3.8: Force and normalized force coefficient on  $1\text{ m} \times 1\text{ m}$  net panels in current condition. (Upper: drag forces over mean incoming velocity. Under: normalized drag coefficients over Reynolds number.) The dots are experimental results and curves are theoretical prediction.

In figure 3.10, the empty circles are original experimental results; the filled circles are experimental results after modification; solid lines are theoretical predictions. Drag coefficient is plot-

ted over Reynolds number. The modified drag coefficient is derived from drag force divided by modified velocity profile. The discrepancy for drag coefficient between the experimental values and theoretical ones has the same result as it for drag force.

Figure 3.11 gives the relative error of drag force between theoretical prediction and experimental result. The differences between them become much smaller after implemented the modified velocity profile, and with the increase of speed, the error is getting even smaller. From above one can conclude that the frame does have a non-negligible effect on the drag force on net during the net panel towing test. Since the net panel has to be towed with the frame, the frame effect should be carefully studied.

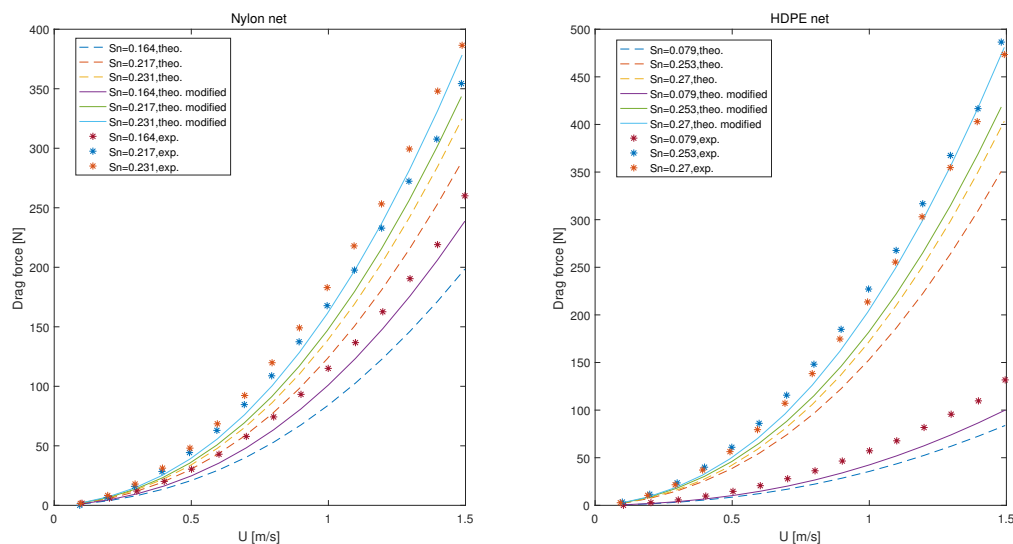


Figure 3.9: Drag forces over mean incoming velocity after applying the modified velocity profile. Asterisks are experimental data; Dash lines are theoretical predictions without modification; Solid lines are predictions with modification.

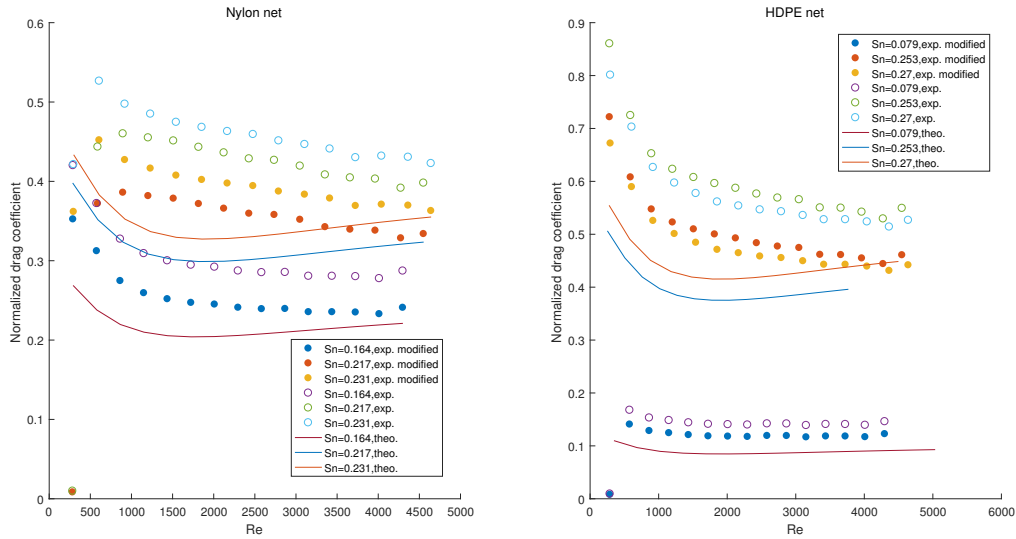


Figure 3.10: Normalized drag coefficient over Reynolds number after applying the modified velocity profile. Empty circles are original experimental results; Filled circles are experimental results after modification; Solid lines are theoretical predictions.

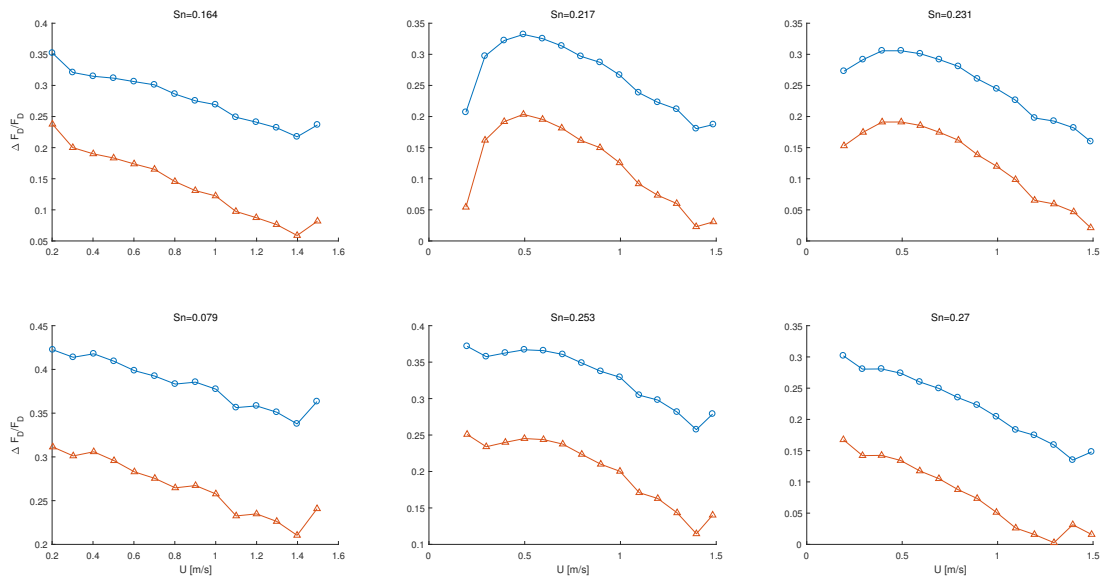


Figure 3.11: Relative error of drag force between theoretical prediction and Experimental results. Blue curve: original theoretical prediction and experimental results. Red curve: modified theoretical prediction and experimental results

### 3.2.2 Wave Only

The nets are fixed in the middle of the tank and tested under different wave periods ( $T$ ), from 0.8s to 1.8s, with a step of 0.2s, which means from 4.8s to 12s in full scale, and wave steepness ( $H/\lambda$ ), which are 1/60, 1/40, 1/20 respectively. That is to say, for each net there are 18 tests. Table 3.2 is the wave only condition test matrix. An example of the time series of wave force is presented in figure 3.12. For each wave period, the wave was made to have a package of 60 periods including 5 ramps up and 5 ramps down and between each package there is a 180-second rest. The wave period of the package in figure 3.12 is 0.8s and the steepness is 1/60. From figure one can observe that the wave realization and the wave force behave well in the tank but there is a non-zero mean offset, which comes from the effect of the environment. The mean offset will affect the accuracy of the force results. Therefore, the mean offset should be filtered before the data being processed.

Table 3.2: Wave only test matrix, showing wave period, steepness for nets with three solidity ratios

Solidity ratio, $S_n$	Wave steepness, $H/\lambda$		
	1/60	1/40	1/20
0.217	0.8-1.8s	0.8-1.8s	0.8-1.8s
0.231	0.8-1.8s	0.8-1.8s	0.8-1.8s
0.253	0.8-1.8s	0.8-1.8s	0.8-1.8s

Figure 3.13 shows the mean wave force amplitude on  $1m \times 1m$  net panels in wave condition. Comparing with the current force, the wave force is relatively much smaller (one can compare the wave force magnitude with that in current condition), which indicates that the wave impact on the net is insignificant and current force is dominating. This is especially for nets under small steepness (i.e.  $H/\lambda = 1/60$  and  $H/\lambda = 1/40$  in this case). Under the same wave period, higher steepness gives higher wave force amplitude. For  $H/\lambda=1/20$ , the wave force amplitude increase more rapidly with the wave period than. For nylon nets (see the right two figures in figure 3.13), at the same wave period and the same steepness, a higher solidity ratio gives a higher wave force amplitude, even though it is not obvious for steepness=1/40 and 1/60. For HDPE net (see first left figure in figure 3.13), the higher solidity ratio instead gives a smaller wave force amplitude

relative to that for nylon nets. The reason may lie in the rigidity of net with different materials. HDPE net which has a large stiffness is much easier to break waves. The broken waves thus result in smaller resistance forces on the net. Nylon net on the contrary, will deform when suffering large waves, and the sensor feels an extra tension from the net deformation. There is a point missing for the wave force on HDPE net at  $H/\lambda = 1/20$  and at  $T=1.8s$ , which is due to the measurement error. However, if one makes a 4<sup>th</sup> order polynomial curve fitting, the wave force amplitude can be predicted within a reasonable range.

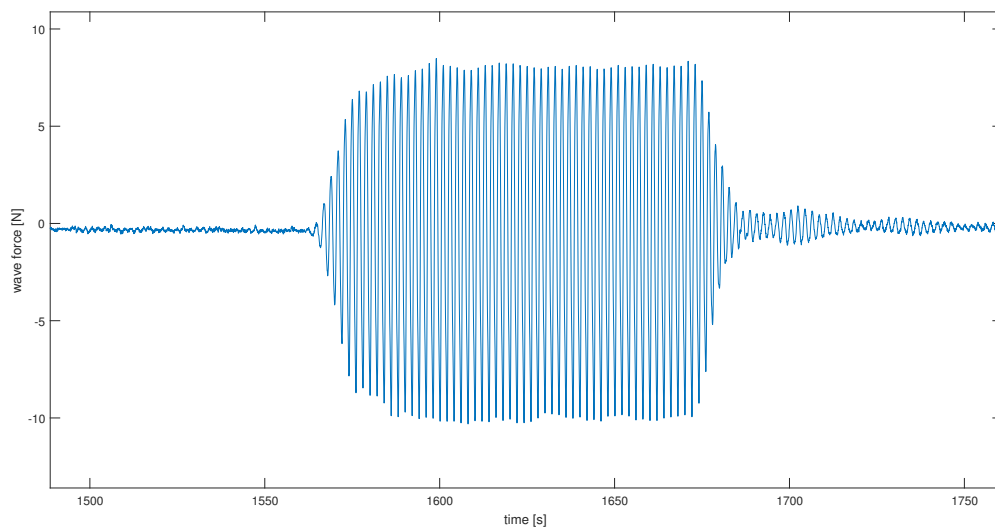


Figure 3.12: Time series of wave force for HDPE net with  $Sn = 0.253$ , and  $d_w = 19mm$ . For this case, the wave period  $T=0.8s$ , and the steepness  $H/\lambda = 1/40$ .

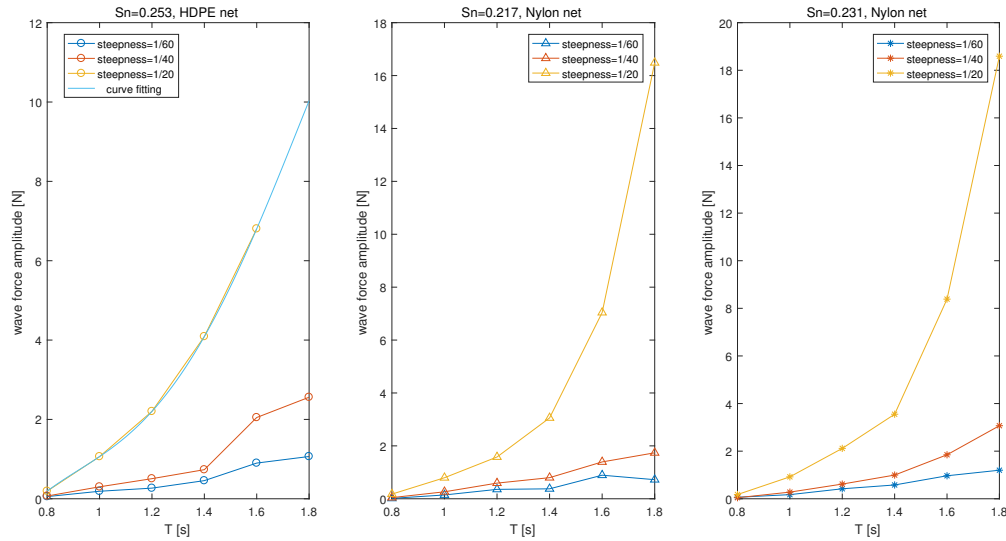


Figure 3.13: Mean wave force amplitude on  $1m \times 1m$  net panels in wave condition.  $T$ =wave period. Steepness= $H/\lambda$ ,  $H$ =wave height,  $\lambda$ =wave length.

The mean wave forces for different nets in wave only condition are presented in figure 3.14. For net with lower solidity ratio and in smaller wave steepness, the mean wave force is very small, which can be negligible while for net with large solidity ratio in large wave steepness and wave period, the mean wave force can be higher, around 16% of the force amplitude (see the mark in figure 3.14). Ideally, there will be no mean wave force on net in regular wave according to the linear wave theory. However, the mean wave force here proves that the wave is not perfectly regular. Another reason for the non-zero mean wave can be the seiching of the tank. Seiching will always happen in a closed tank. Due to seiching, a slowly varying current exists in the middle of the tank (the net was right fixed in the middle of the tank), adding to the resistance force on net panel. Figure 3.15 proves the existance of seiching. The seiching period of the towing tank is  $T_{seich} = 2L_{tank}/\sqrt{gh} \approx 18s$  and one can observe a slow varying oscillation of around 18s period as well.

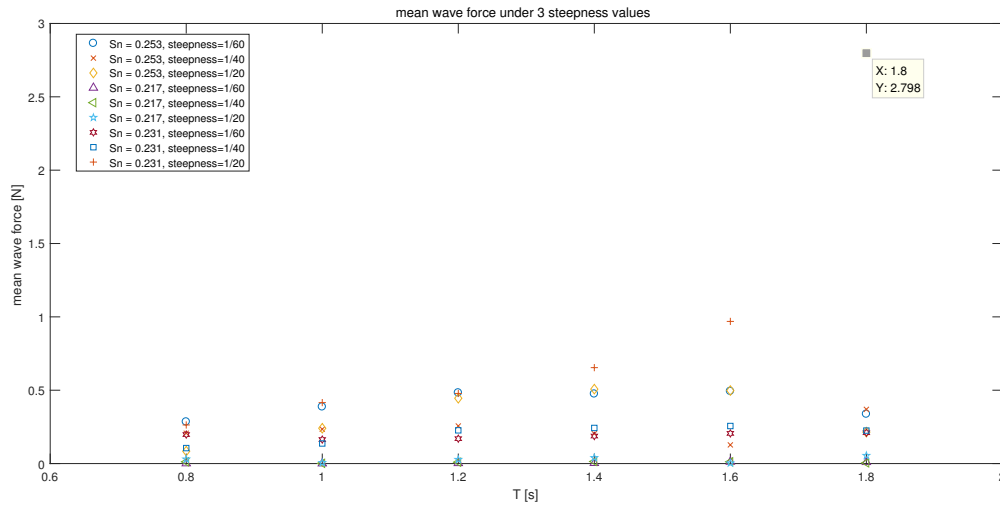


Figure 3.14: Mean wave force on  $1\text{ m} \times 1\text{ m}$  net panels in wave only condition.  $T$ =wave period. Steepness= $H/\lambda$ ,  $H$ =wave height,  $\lambda$ =wave length.

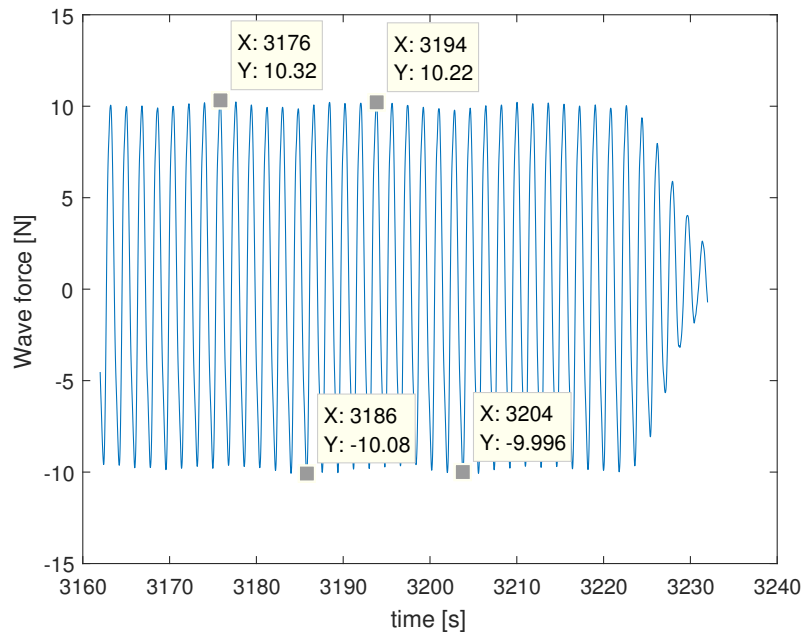


Figure 3.15: Time series of filtered wave force for net with  $S_n = 0.217$ . In this case, wave period  $T=1.6\text{ s}$ , wave steepness  $H/\lambda=1/40$

### 3.2.3 Current and Wave

In this situation, the net was towed at the speed of 0.1m/s and 0.2m/s, and there were waves with period from 5/6s to 10/6s with a step of 1/6s, according to the wave period in full scale which is from 5s to 10s. That is to say, for each net there are 12 tests. Table 3.3 gives the current with wave test matrix. Figure 3.16 illustrates the time series of wave and current force for HDPE net with  $S_n=0.253$ . The time series are for wave period  $T = \frac{5}{6}$ s and steepness  $H/\lambda = \frac{1}{40}$ .  $U_\infty$  is incoming flow velocity. The wave period during the time region in figure 3.16 is  $T=\frac{5}{6}$ s and the steepness is 1/40. The blue curve is for  $U_\infty = 0.1\text{ m/s}$  and the red one is for  $U_\infty = 0.2\text{ m/s}$ . The force oscillation is smaller at higher towing speed.

Table 3.3: Current with wave test matrix, showing towing speed, wave period, steepness for nets with three solidity ratios

Solidity ratio, $S_n$	Current, $U_\infty$ (m/s)	Wave steepness, $H/\lambda$	
		1/40	1/20
0.217	0.1	5/6-10/6s	5/6-10/6s
	0.2	5/6-10/6s	5/6-10/6s
0.231	0.1	5/6-10/6s	5/6-10/6s
	0.2	5/6-10/6s	5/6-10/6s
0.253	0.1	5/6-10/6s	5/6-10/6s
	0.2	5/6-10/6s	5/6-10/6s

Figure 3.17 depicts the mean force in current with wave condition. The force at  $T = 0$ s is the drag force obtained from current only condition. The mean force increases gradually with the wave period. Higher solidity ratio gives a higher mean force. A doubled incoming flow velocity gives an almost squared mean force while the steepness effect on the mean force is not significant. This again proves that current is more important than the wave when considering the drag force on net panels.

Figure 3.18 and figure 3.19 show the force amplitude on nets. The first order force amplitude increases almost linearly with the wave period, and higher solidity ratio gives higher force amplitude. A doubled current velocity gives an almost doubled first order force amplitude and the impact from the steepness this time is more obvious (A doubled steepness gives an at least dou-

bled force amplitude), which means for force amplitude, the current and wave are both important. The second order force amplitude comes from the second order frequency of the waves. It is much smaller than that of first order. There is a drop for the second order force amplitude for each net when it develops with the wave period. This may due to some cancellation effects.

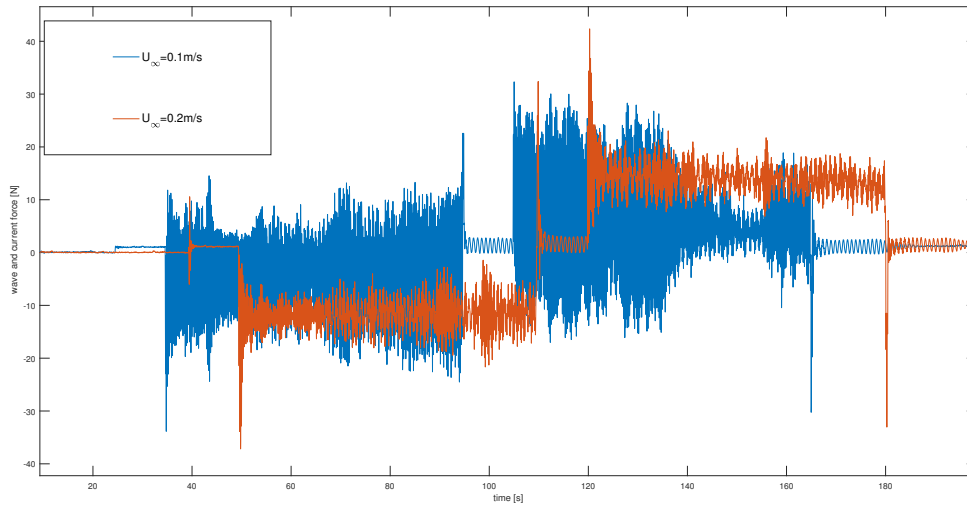


Figure 3.16: Time series of wave and current force for HDPE net with solidity ratio  $S_n=0.253$ . The time series are for wave period  $T = \frac{5}{6}$  s and steepness  $H/\lambda = \frac{1}{40}$ .  $H$  is the wave height, and  $\lambda$  is the wave length.  $U_\infty$  is incoming flow velocity.

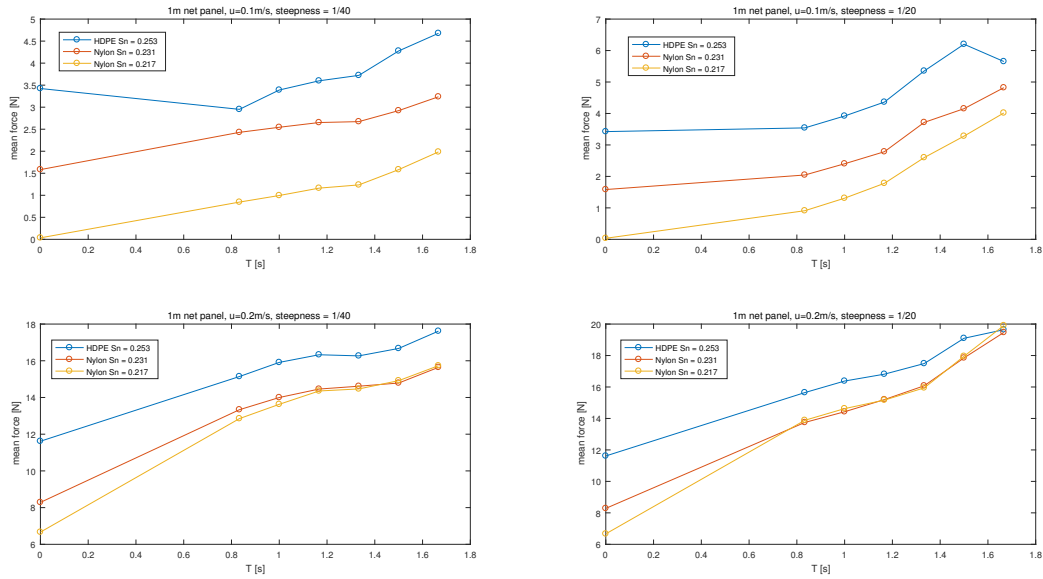


Figure 3.17: Mean force on  $1\text{ m} \times 1\text{ m}$  net panels in current and wave condition,  $u =$  current speed,  $T =$  wave period. Steepness  $= H/\lambda$ , where  $H$  is the wave height and  $\lambda$  is the wave length.

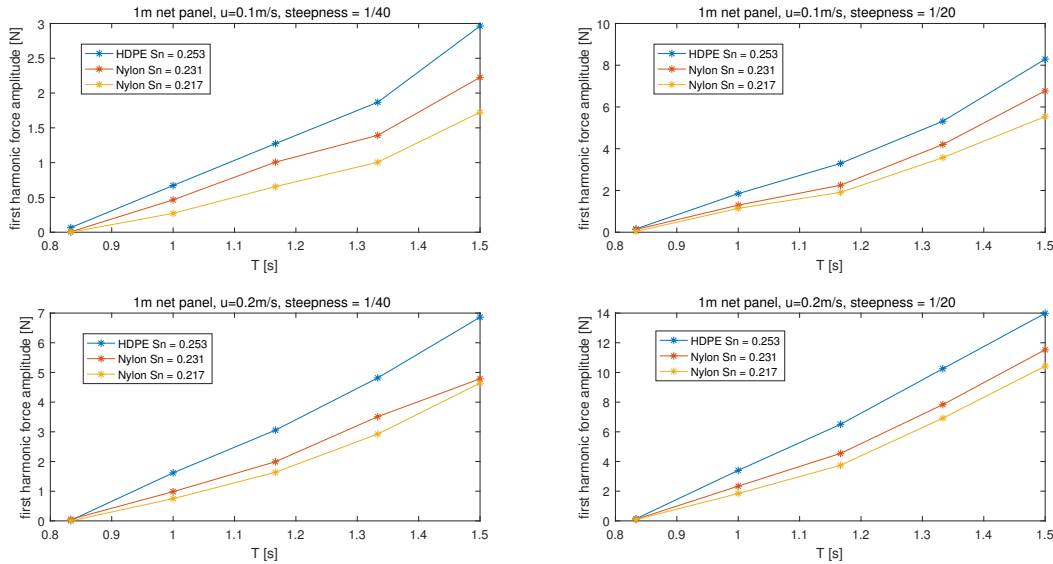


Figure 3.18: First order force amplitude on  $1\text{ m} \times 1\text{ m}$  net panels in current and wave condition,  $u =$  current speed,  $T =$  wave period. Steepness  $= H/\lambda$ , where  $H$  is the wave height and  $\lambda$  is the wave length.

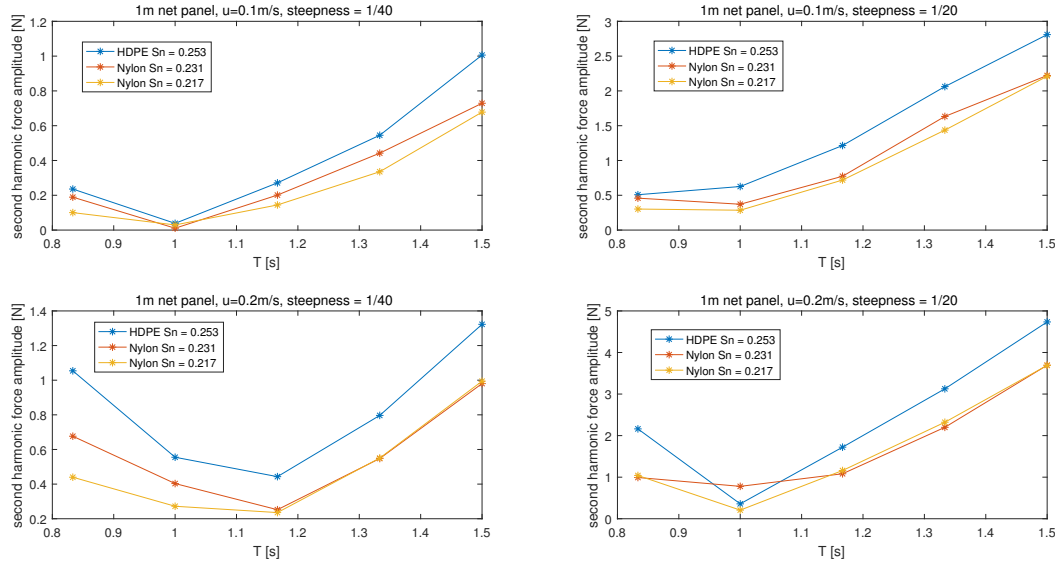


Figure 3.19: Second order force amplitude on  $1\text{m} \times 1\text{m}$  net panels in current with wave condition,  $u$ =current speed,  $T$ =wave period. Steepness =  $H/\lambda$ , where  $H$  is the wave height and  $\lambda$  is the wave length.

### 3.3 Error and Uncertainty

Although the lab tests are designed to be as much precise as possible, there are errors and uncertainties inevitably. Errors and uncertainties can be mainly concluded as following:

- Uncertainty in measuring solidity ratio and twine diameter. As discussed above, the solidity ratio was measured with GIMP technique and the twine diameter and half mask length are measured by vernier caliper. The GIMP technique gives a poor solution when the net is not pure black or white or there are shadow and reflect light on the net. Figure 3.20 shows three estimated  $S_n$  values for the same net, and the largest deviation is 7.7%. Thus, it was decided to take photos at least for 3 times for the same net and averaged value was adopted to reduce the uncertainty from solidity ratio.
- Uncertainty from net deformation during the towing test. The net was stretched onto the frame as tightly as possible to ensure no large deformation during towing. However, slack is inevitable after repeated tests for the same net, especially for nylon nets. It is hard

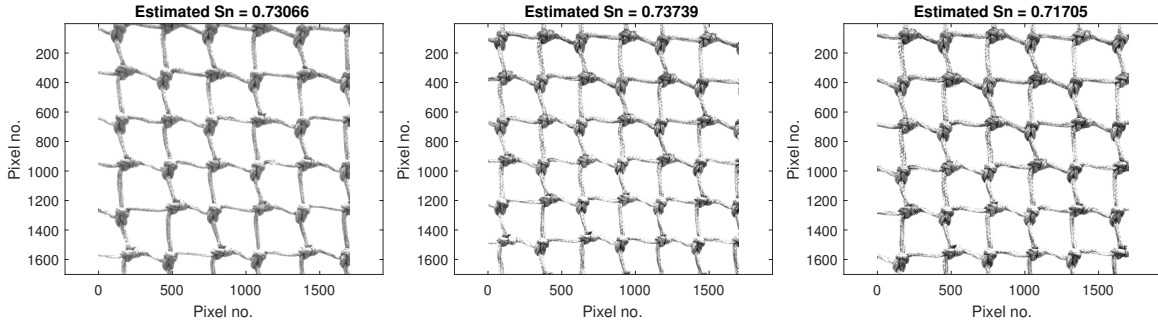


Figure 3.20: Comparison of estimated solidity ratios by GIMP for the same net. The net has a final solidity ratio value of  $S_n = 0.27$ .

to quantify the net deformation. For nylon net with  $S_n = 0.217$ , the largest difference between slack and tight condition is  $22N$  (see figure 3.21), i.e. the force on slack net can be at most 4.3% higher than the force after the net was re-stretched.

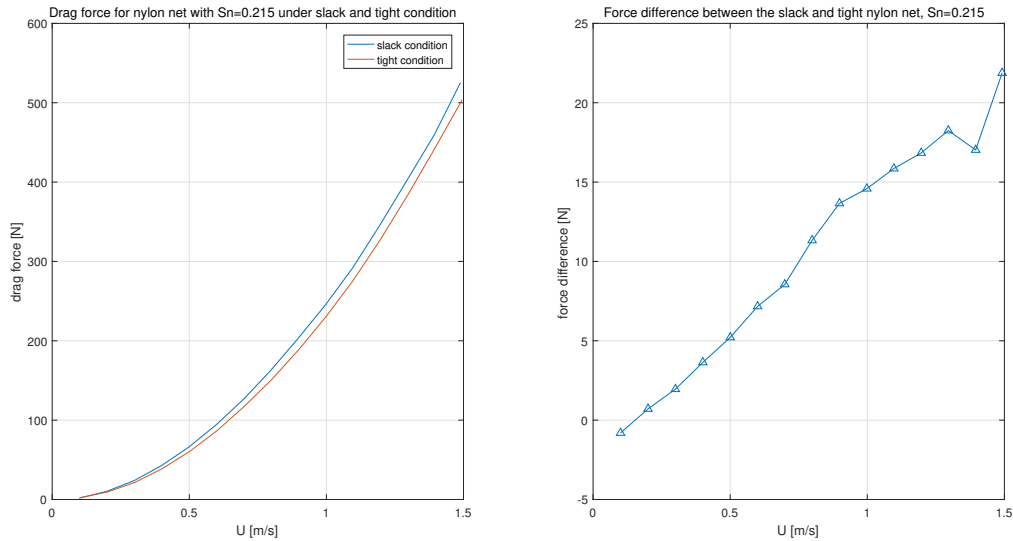


Figure 3.21: Comparison of drag forces on nylon net with  $S_n = 0.217$  under slack and tight condition. Left: drag forces over incoming flow velocity  $U$ ; Blue curve shows the drag force on the net when it was in slack condition; Red curve shows the drag force on the net when it was re-stretched to a tight condition. Right: force difference ( $F_D^{slack} - F_D^{tight}$ ) over incoming flow velocity  $U$ .

- Errors in calculation of mean towing force. The towing force showed unstable before the carriage was stopped when the net was towed at a higher speed. An example of the time

series of  $F_x$  is shown below (see figure 3.22), in which plotted the resistance forces on three nets at speed of 1.4m/s and 1.5m/s. The forces did not develop til stable before the net was stopped towing, which causes troubles for calculating the mean towing force. The biggest uncertainty bound could be more than 10%.

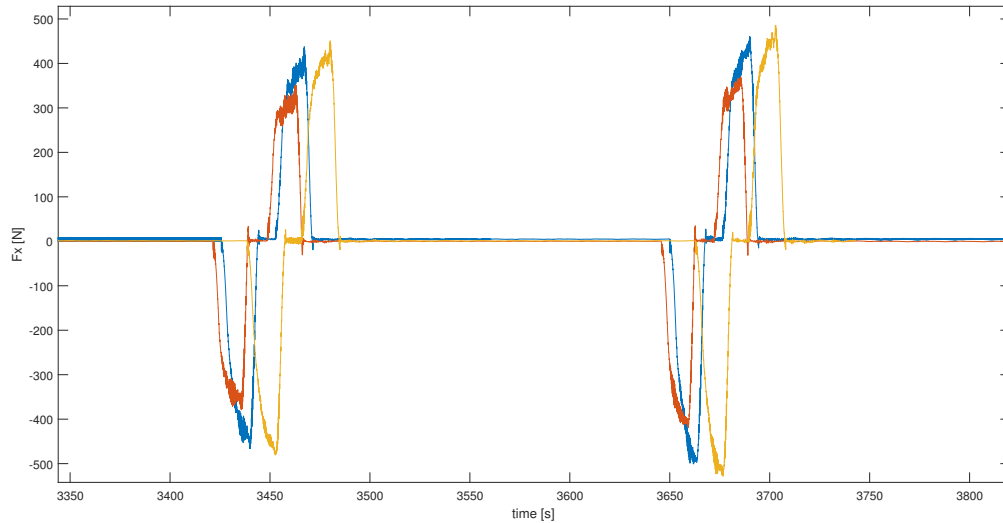


Figure 3.22: Time series of drag forces for three nets under current speed at 1.4m/s and 1.5m/s. Blue curve: net with  $S_n=0.217$ . Red curve: net with  $S_n=0.164$ . Yellow curve: net with  $S_n=0.231$ .  $F_x$ : resistance force in x direction (normal direction to the net panel).

- Uncertainty from non-zero mean offset. It was observed that there was a very small (approximately 1N) non-zero mean offset as long as the machine started, no matter if the carriage is started. Since it is much smaller comparing to the final drag force on net, the non-zero offset is negligible.
- Uncertainty in wave height. The actual wave height is not exactly the same as one planned. The wave maker generates waves which are designed in advance. The designed wave motion can be plotted in Matlab and the actual waves are measured (see figure 3.23). For waves with large wave height and wave period, the measured results are deviated from the planned ones. This is due to the limitation of wave flapper.
- Uncertainty from empty frame force. The force on empty frame was tested separately, and the mean towing velocity corresponding to each mean towing force could be different.

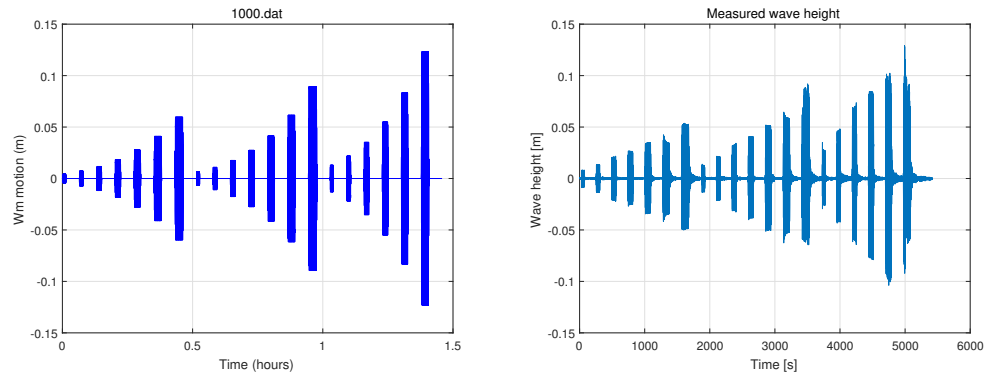


Figure 3.23: Comparison of designed wave height and measured wave height. Left: designed wave motion plot generated in Matlab. Right: wave motion measured from wave probes.

In other words, the measured mean towing speed is slightly different every time, which results in uncertainty of mean towing force. See table 3.4 for their difference.

- The wave is assumed to be regular, which means only first order frequency exists. However, the wave has second order frequency. For nylon nets at high wave period and high steepness, there are higher order frequencies (see figure B.3 in appendix B for instance). Besides, for nets in current and wave condition, there is noise at higher frequency. The power spectral density of forces can be found in appendix B.

Table 3.4: The measured average towing speeds for different tests

	standard towing speed [m/s]			
	0.1	0.5	1.0	1.5
	measured towing speed [m/s]			
empty frame test	0.0995	0.4994	0.9994	1.4981
test for net with $S_n=0.217$	0.0932	0.4934	0.9953	1.4851
test for net with $S_n=0.27$	0.0920	0.4919	0.9938	1.4924

### 3.4 Comments

- One of the main uncertainty lies in estimating the solidity ratio. No matter which method cannot give a 100% answer. Thus an error bound should be left for accounting the uncer-

tainty from solidity ratio.

- The empty frame has a large effect on the drag force of the net panel, especially for net in current only condition. The main effect comes from that the frame change the flow field near it and lead to a modified velocity profile in front of the net. Therefore, if one applies the modified velocity profile, the theoretical results will be significantly raised and will be closer to the experimental results. To conclude, the frame effect should be carefully studied when doing the net panel towing test. An improvement is expected for frame which has a more streamlined body and smaller effect on the net.
- Comparing with the wave, the current has a dominating contribution on the drag force. One should focus more on net in the current condition. However, net will also be potentially damaged if it suffer extreme wave condition.
- The wave gives a first harmonic force as well as second harmonic force, which could not be neglected. Higher order harmonic force also exists, but it is not studied in this thesis.
- Uncertainties come from both factitious and inherent aspects. The uncertainties should be cautiously considered since some of them will lead to large discrepancy.

# Chapter 4

## Numerical Investigation

### 4.1 Numerical Set-up

#### 4.1.1 Description of Model Set-up

The numerical simulation in this thesis is realized in the framework of the open source computational fluid dynamics toolbox OpenFOAM with version 4.1 ([Greenshields \(2015\)](#)). The porous media model was proposed to solve the flow characteristics through and around a net panel. It was set up as porous medium in single phase flow and two phase flow. The porous medium in single phase flow was solved by a transient single phase solver and the porous medium in two phase flow was solved by a multiphase solver for incompressible, isothermal and immiscible fluids using volume of fluid (VOF) method. The model was applied as laminar since the quadratic drag resistance coefficient derived from experimental force and rational force models will have already taken all the dissipation effects into account.

The 2D porous media model was set up in two cases: top view and side view, referring to (a) and (b) in figure [4.1](#). The sketches of domains are also depicted in it. The width of the porous media was set to be 0.05m, which is a commonly used value for porous media. The length of the porous media (0.95m in top view and 0.85m in side view) is decided according to the net panel size in experiment, which is  $0.85 \times 0.95 m^2$ .

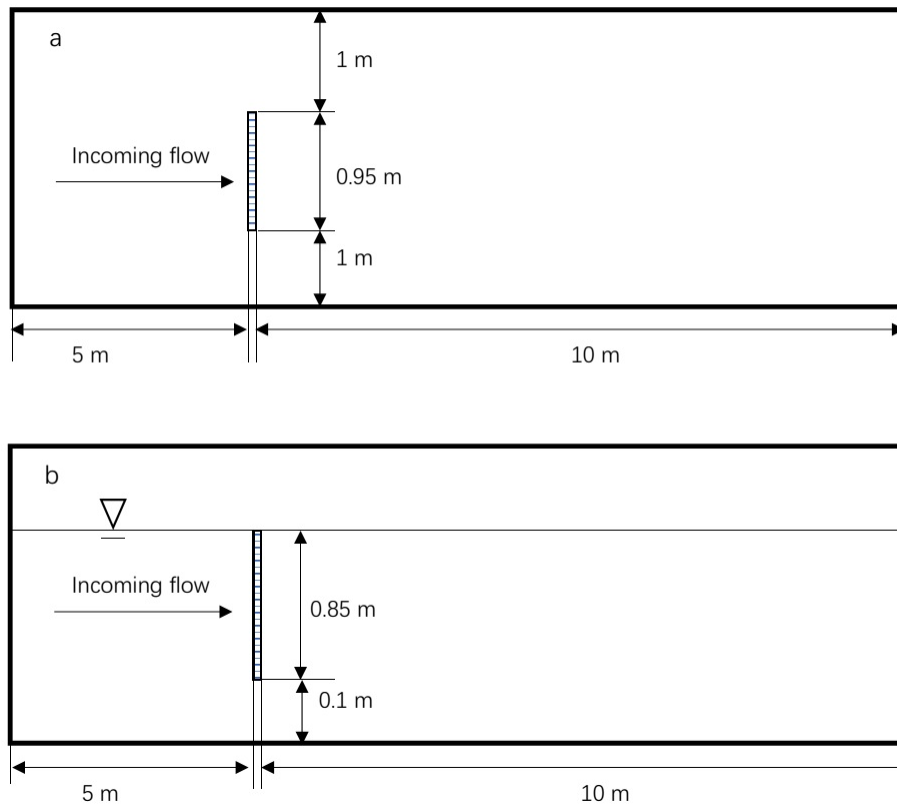


Figure 4.1: Sketch of the domain for 2D numerical model in two cases. (a) Top view. (b) Side view. The shadow area is the porous media with 0.05m width.

The top view case describes the situation of the net in the towing tank from a bird's eye view. It was solved by the transient single phase solver. The up and down side of the domain was set to be slip wall; the front side is inlet with fixed uniform flow, and the back side is outlet with zero gradient boundary condition. A multi-phase flow solver was applied to solve the side view case, which describes the situation of net from the side view. Thus, gravity is considered in this case. The porous medium was fully submerged under water. The inlet(front side) and outlet(back side) were set to be with the same fixed flow velocity to ensure the mass conservation. The bottom is slip wall and the top is atmosphere. However, only current condition has been modelled in this thesis (no wave was implemented into the cases), so the wave properties were not inputted for porous media in side view case.

The realizations in OpenFOAM are presented in figure 4.3, in which (a) and (b) are the velocity

and pressure profile of net with  $S_n = 0.217$  and incoming flow velocity  $U_\infty = 0.5 m/s$  from a top view, and (c) and (d) are alpha water and pressure profile of net with  $S_n = 0.217$  and incoming flow velocity  $U_\infty = 1 m/s$  from a side view. In figure 4.3 (c), there is surface elevation just behind the net, which is caused by the disturbance from the net. This leads to the oscillation of the drag force. And this phenomenon is exactly the same situation in practical experiments (see figure 4.2). Just behind the net, the water surface was raised and turbulence occurs, and then dropped down into a trough and raised again.

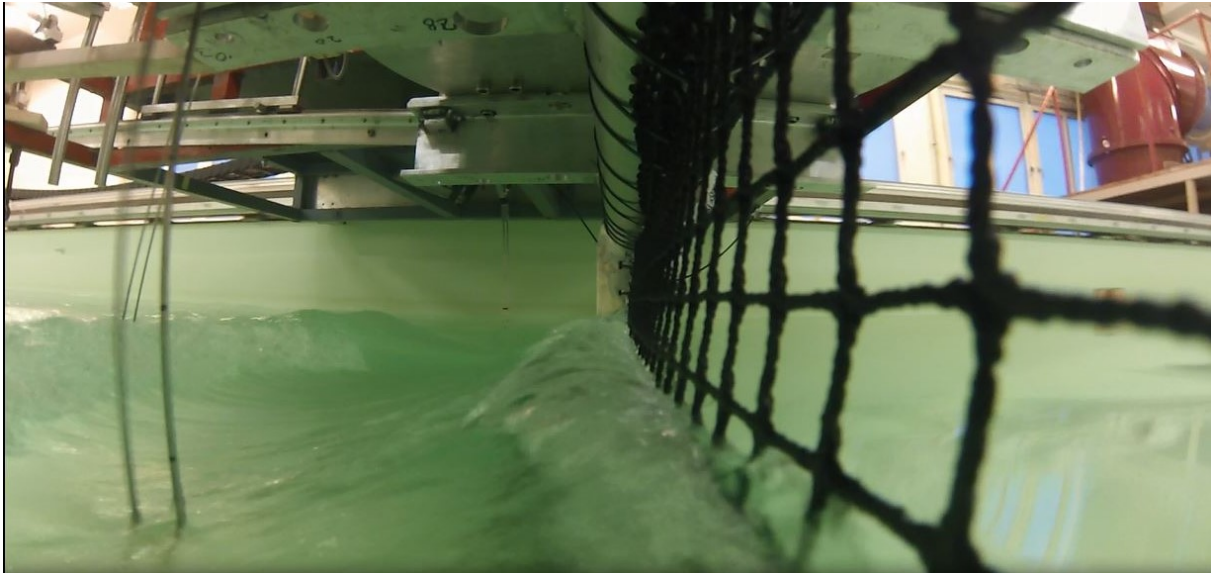


Figure 4.2: Screenshot from the video about the surface elevation behind the net during towing process.

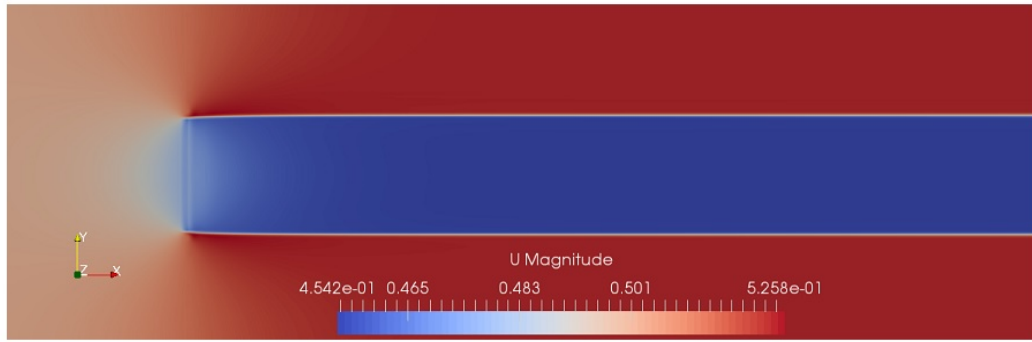
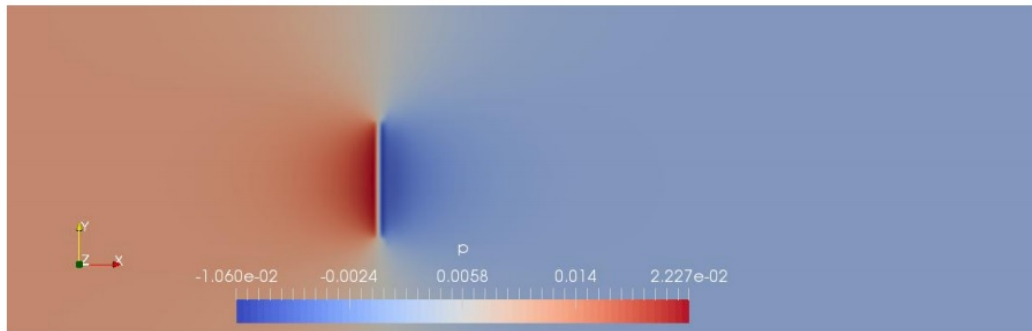
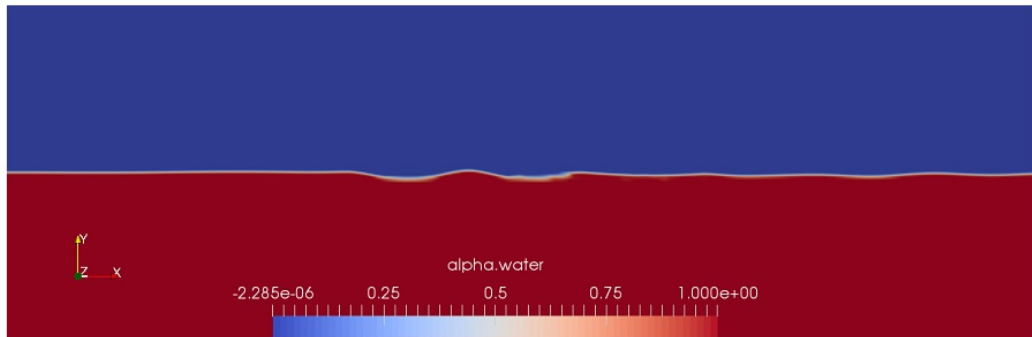
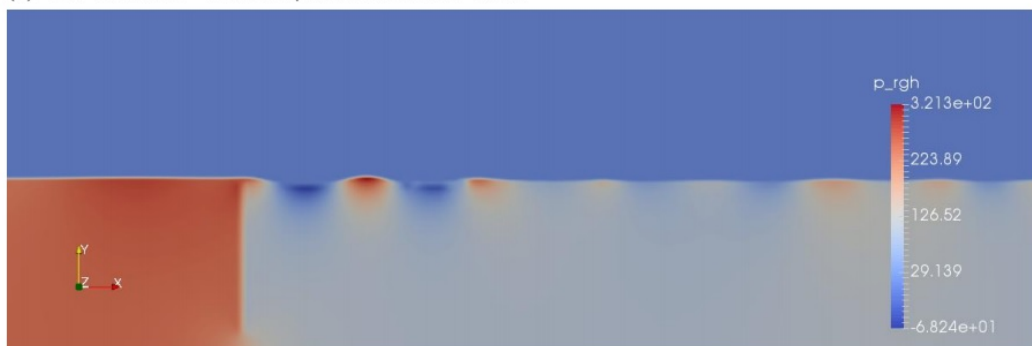
(a)  $S_n=0.217$ ,  $U=0.5\text{m/s}$ , U profile, top view.(b)  $S_n=0.217$ ,  $U=0.5\text{m/s}$ , P profile, top view.(c)  $S_n=0.217$ ,  $U=1\text{m/s}$ , alpha water, side view.(d)  $S_n=0.217$ ,  $U=1\text{m/s}$ , P profile, side view.

Figure 4.3: Realization in OpenFOAM. (a) and (b) are the velocity and pressure profile of net with  $S_n = 0.217$  and incoming flow velocity  $U_\infty = 0.5\text{m/s}$  from a top view, and (c) and (d) are phase and pressure profile of net with  $S_n = 0.217$  and incoming flow velocity  $U_\infty = 1\text{m/s}$  from a side view.

### 4.1.2 Convergence Test

Size of mesh is very important near and around the porous medium since one needs to integrate the velocity and pressure distribution around the porous medium to get the total drag force on it. They should be carefully captured with very fine mesh. Therefore, a series of preliminary tests were run to examine the convergence in time domain. Hexahedral mesh was applied in the simulation. The grading in horizontal direction (along the length of the domain) was set to be 1:6 and that in vertical direction (along the width of the domain) was set to be 1:4 so that near the porous medium one has the finest mesh and at the boundary of the domain the mesh is coarser.

4 mesh schemes were planned to be tested. They are, according to the porous medium thickness which is 50mm, grid size of 50/1 mm, 50/2 mm, 50/3 mm and 50/4 mm. In other words, along the thickness of porous medium, cell number  $N=1$ ,  $N=2$ ,  $N=3$  and  $N=4$  are chosen to be put on. Figure 4.4 illustrates the time series of unit drag forces for 4 mesh schemes. The porous medium in this case has a volume of  $0.1\text{ m} \times 0.85\text{ m} \times 0.05\text{ m}$  and the incoming flow velocity is 0.5m/s. This is the case in side view. For  $N=1$ , the force has an oscillation around 1N after the simulation is steady and it is still divergent at  $t=100\text{ s}$ . The result for  $N=2$  gives much better steady trend. The largest oscillation is only around 0.2N after simulation is steady.  $N=3$  gives 0.07N (2%) force oscillation at most and For  $N=4$ , the force oscillation shows a better convergence but the computational time is too long. If one looks at the convergence trend (see figure 4.5), he will find that the force difference between  $N=3$  and  $N=4$  has been reduced to 0.5%, which is an acceptable value of error. Thus, to balance the computational time and calculation accuracy, mesh scheme  $N=3$  was applied in the following tests.

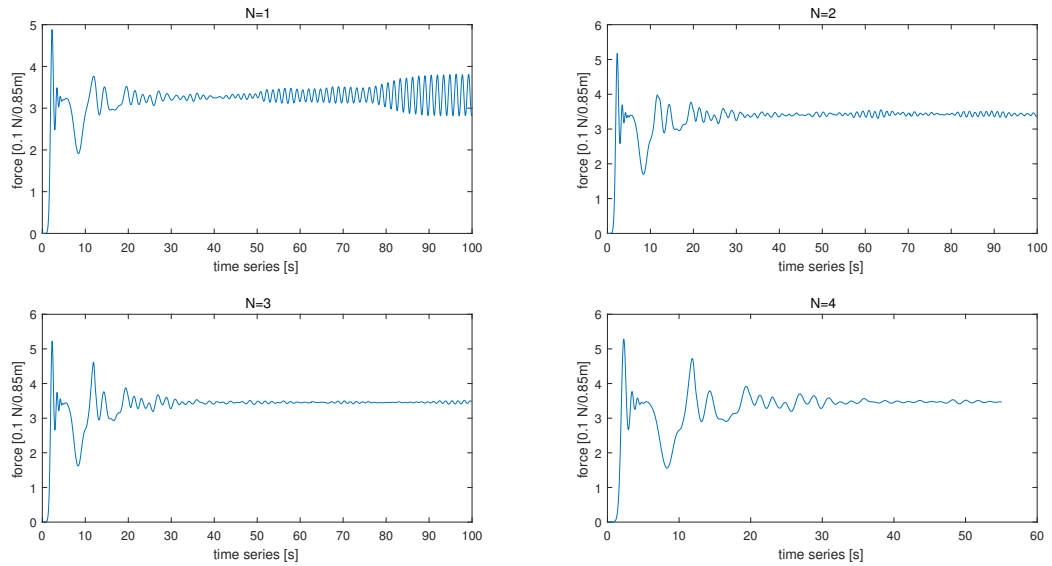


Figure 4.4: Time series of drag forces for 4 mesh schemes.  $N$ =cell number along the thickness of the porous medium. The porous medium in this case has a volume of  $0.1m \times 0.85m \times 0.05m$ . Incoming flow velocity= $0.5m/s$ . Side view.

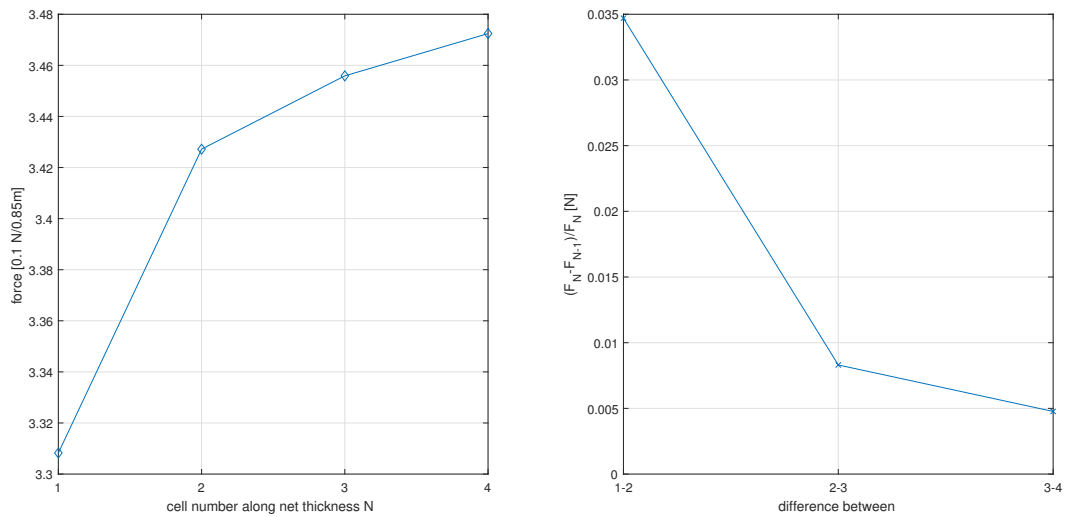


Figure 4.5: Convergence trend of drag forces for 4 mesh schemes.  $N$ =cell number along the thickness of the porous medium. The porous medium in this case has a volume of  $0.1m \times 0.85m \times 0.05m$ . Incoming flow velocity= $0.5m/s$ . Side view.

## 4.2 Results and Discussion

In this thesis, nets with three different solidity ratios ( $S_n = 0.164$ ,  $S_n = 0.217$ ,  $S_n = 0.231$ ) under three incoming flow velocities ( $U=0.5\text{m/s}$ ,  $U=1.0\text{m/s}$ ,  $U=1.5\text{m/s}$ ) will be tested, and the quadratic drag resistance coefficient will be derived from three theories, i.e. screen type force model, modified Morison force model, and direct experimental force. The detailed numerical simulation scheme is given in table 4.1. It lists the velocities, the solidity ratios and the corresponding quadratic drag resistance coefficients to be tested. The quadratic drag resistance coefficients are calculated according to the principle introduced in chapter 2.

Table 4.1: Numerical test matrix, including net parameter, incoming flow velocity and the corresponding porous resistance coefficients.

		Screen model			Morison model			Experiment		
U [m/s]		0.5	1.0	1.5	0.5	1.0	1.5	0.5	1.0	1.5
Sn=0.164	$C_{11}$	4.13	4.17	4.38	4.25	4.29	4.51	6.02	5.70	5.72
	$C_{22}$		0		1.42	1.43	1.51		0	
	$C_{33}$				1.42	1.43	1.51			
Sn=0.217	$C_{11}$	6.02	6.15	6.48	5.88	6.01	6.32	8.78	8.31	7.80
	$C_{22}$		0		1.80	1.84	1.94		0	
	$C_{33}$				1.80	1.84	1.94			
Sn=0.231	$C_{11}$	6.59	6.75	7.11	6.33	6.49	6.83	9.52	9.06	8.51
	$C_{22}$		0		1.89	1.94	2.04		0	
	$C_{33}$				1.89	1.94	2.04			

Figure 4.6 gives an example of the time series of drag force on porous medium with  $S_n = 0.217$ , of which drag coefficient is derived from experimental forces. The unit of force is given by  $0.1\text{N}/0.85\text{m}$  or  $0.1\text{N}/0.95\text{m}$ , which is according to the volume of the porous medium in top view and side view respectively. The time series from top view shows faster convergence trend and gives more steady force development while case from side view gives a big oscillation at the beginning and requires more time to get steady. The oscillation phenomenon is mainly due to the free surface effect. In reality, the surface elevation due to the disturbance from the moving net

will give the drag force an oscillation. However, the oscillation becomes smaller when the towing speed is increasing. After sometime when the simulation is steady, there will also be surface elevation in front of the net and the free surface level will be raised. This is because the flow speed behind the net is always smaller and there are limited space for higher velocity to exist behind the net. The total momentum behind the porous medium is more likely smaller than the momentum before the porous media. Thus to maintain the momentum conservation, the fluid will be squeezed til the top of the surface and raise the free surface level.

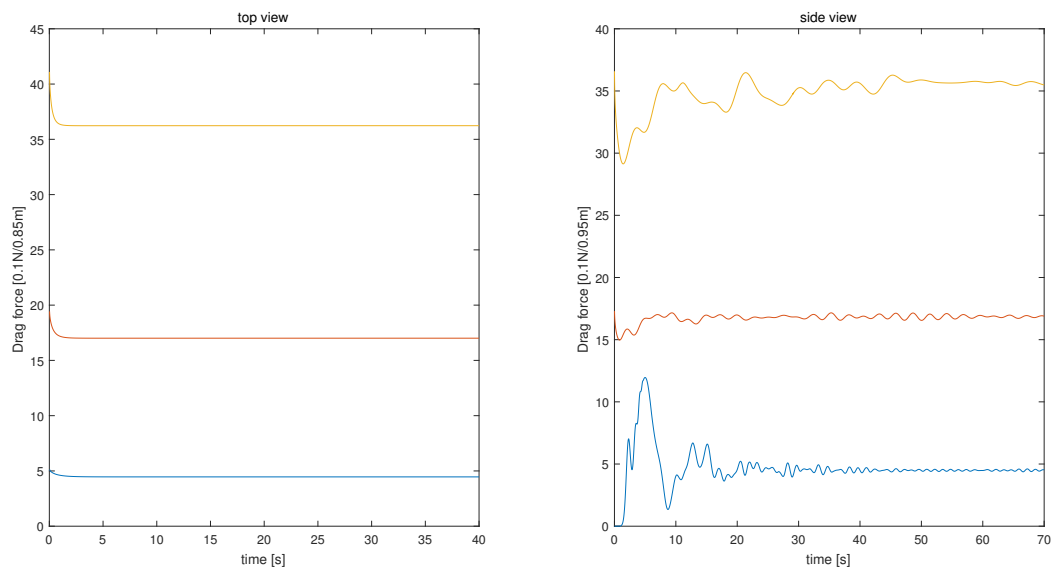


Figure 4.6: Time series of drag force in numerical simulation for net with  $S_n = 0.217$ . Drag coefficient is derived from test results. Left: top view. Right: side view. Blue line: incoming flow velocity=0.5m/s; Red line: incoming flow velocity=1.0m/s; Yellow line: incoming flow velocity=1.5m/s.

Figure 4.7 and figure 4.8 present the velocity and pressure profile for porous medium with  $S_n = 0.217$  from top view. Figure 4.7 is that at the center of the domain along x direction from inlet to outlet. One can find that the pressure will be raised a little just in front of the porous medium. This is because the fluid particles in front of it cannot pass through the porous medium in time due to the velocity reduction behind the porous medium, resulting in an accumulation just in front of it. One can also observe this phenomenon in the experiment. The velocity drop behind the porous medium can be about 10% reduced from the original value. From figure 4.8 one ob-

serves that the pressure behind the porous medium is negative.

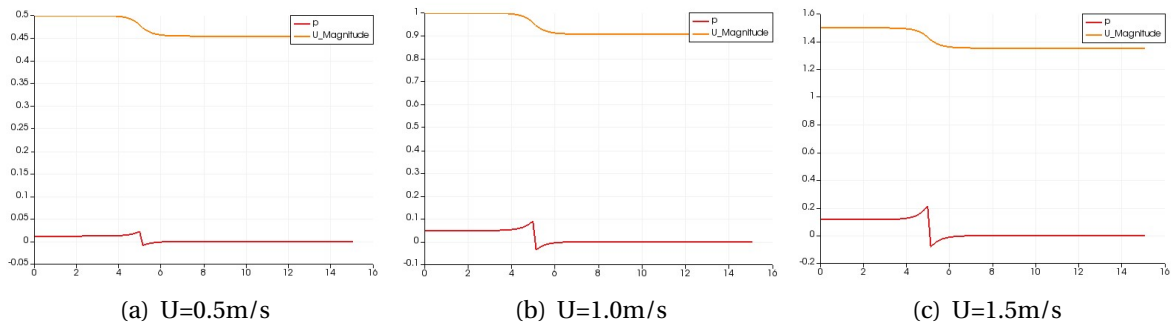


Figure 4.7: Velocity and pressure profile for net with  $S_n=0.217$  from top view at the center of the domain along x direction. horizontal axis: x position from inlet to outlet; vertical axis: velocity or pressure value. (a)  $U=0.5\text{m/s}$ . (b)  $U=1.0\text{m/s}$ . (c)  $U=1.5\text{m/s}$ .

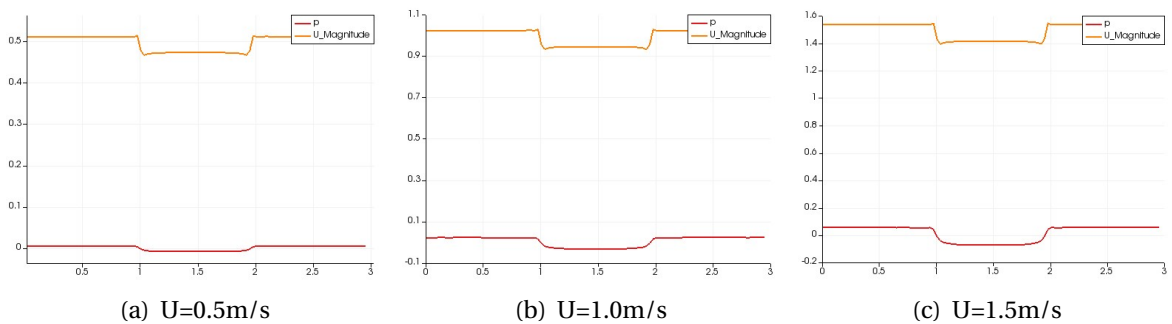


Figure 4.8: Velocity and pressure profile for net with  $S_n=0.217$  from top view just behind the porous medium along y direction. horizontal axis: y position, from down side wall to upper side wall; vertical axis: velocity or pressure value. (a)  $U=0.5\text{m/s}$ . (b)  $U=1.0\text{m/s}$ . (c)  $U=1.5\text{m/s}$ .

Figure 4.9 to figure 4.11 give the velocity and pressure profile for net with  $S_n=0.217$  from side view at the free surface height of the domain along x direction or just behind the porous medium along y direction (the incoming flow velocity is  $0.5\text{m/s}$ ,  $1.0\text{m/s}$ ,  $1.5\text{m/s}$  for three figures respectively). One can also find the surface elevation in front of the porous medium as we mentioned above in figures of U and P profile that are along x direction.

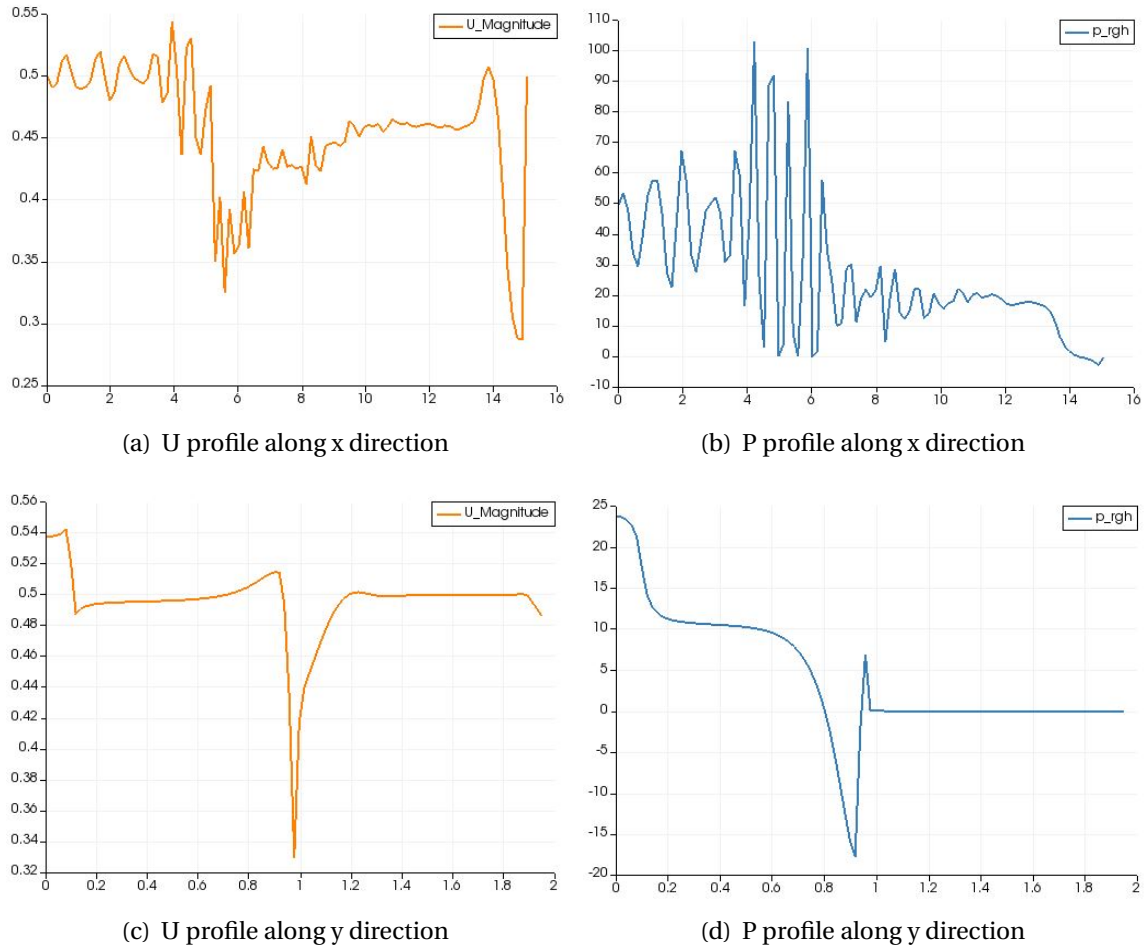


Figure 4.9: Velocity and pressure profile for net with  $S_n=0.217$  at  $U=0.5\text{m/s}$  from side view at the free surface height of the domain along x direction or just behind the porous medium along y direction. horizontal axis: x position from inlet to outlet or y position from bottom to top; vertical axis: velocity or pressure value. (a) U profile along x direction. (b) P profile along x direction. (c) U profile along y direction. (d) P profile along y direction.

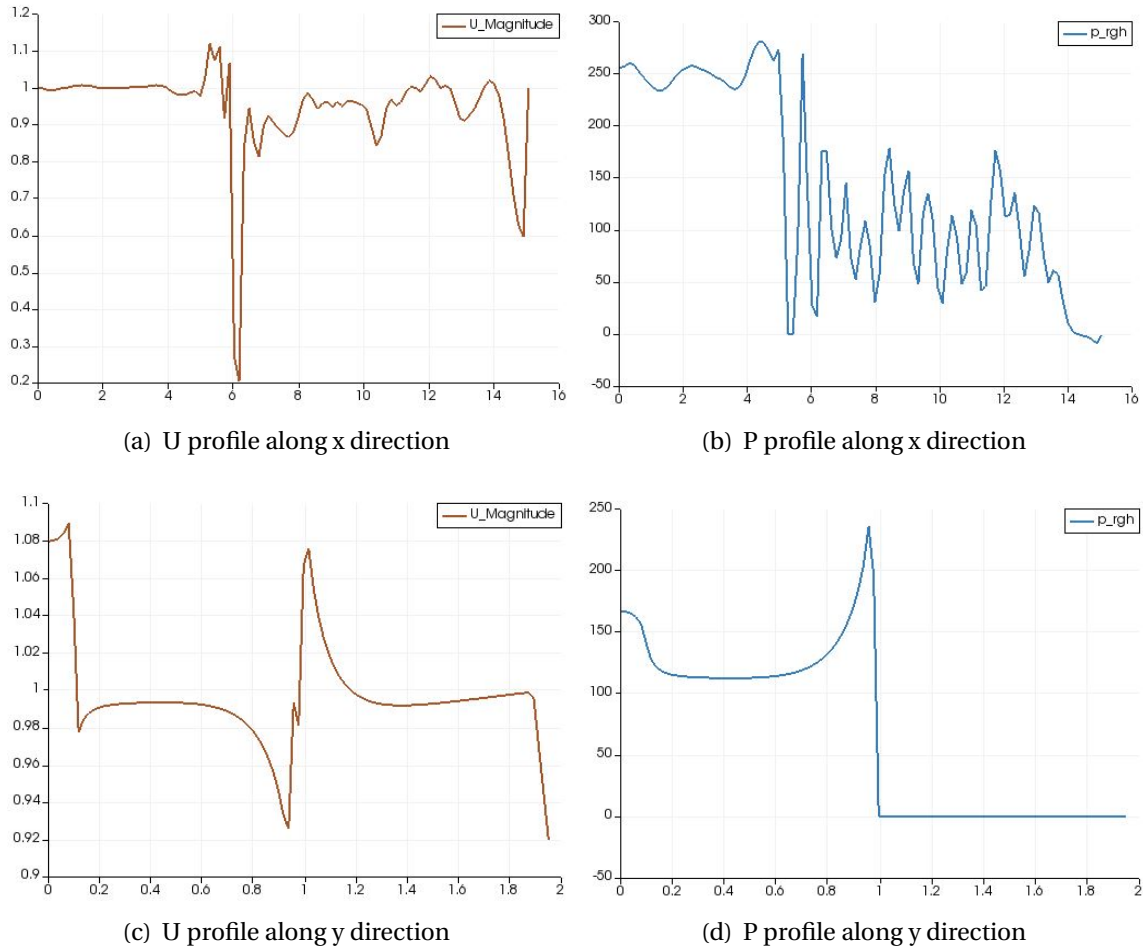


Figure 4.10: Velocity and pressure profile for net with  $S_n=0.217$  at  $U=1.0\text{m/s}$  from side view at the free surface height of the domain along x direction or just behind the porous medium along y direction. horizontal axis: x position from inlet to outlet or y position from bottom to top; vertical axis: velocity or pressure value. (a) U profile along x direction. (b) P profile along x direction. (c) U profile along y direction. (d) P profile along y direction.

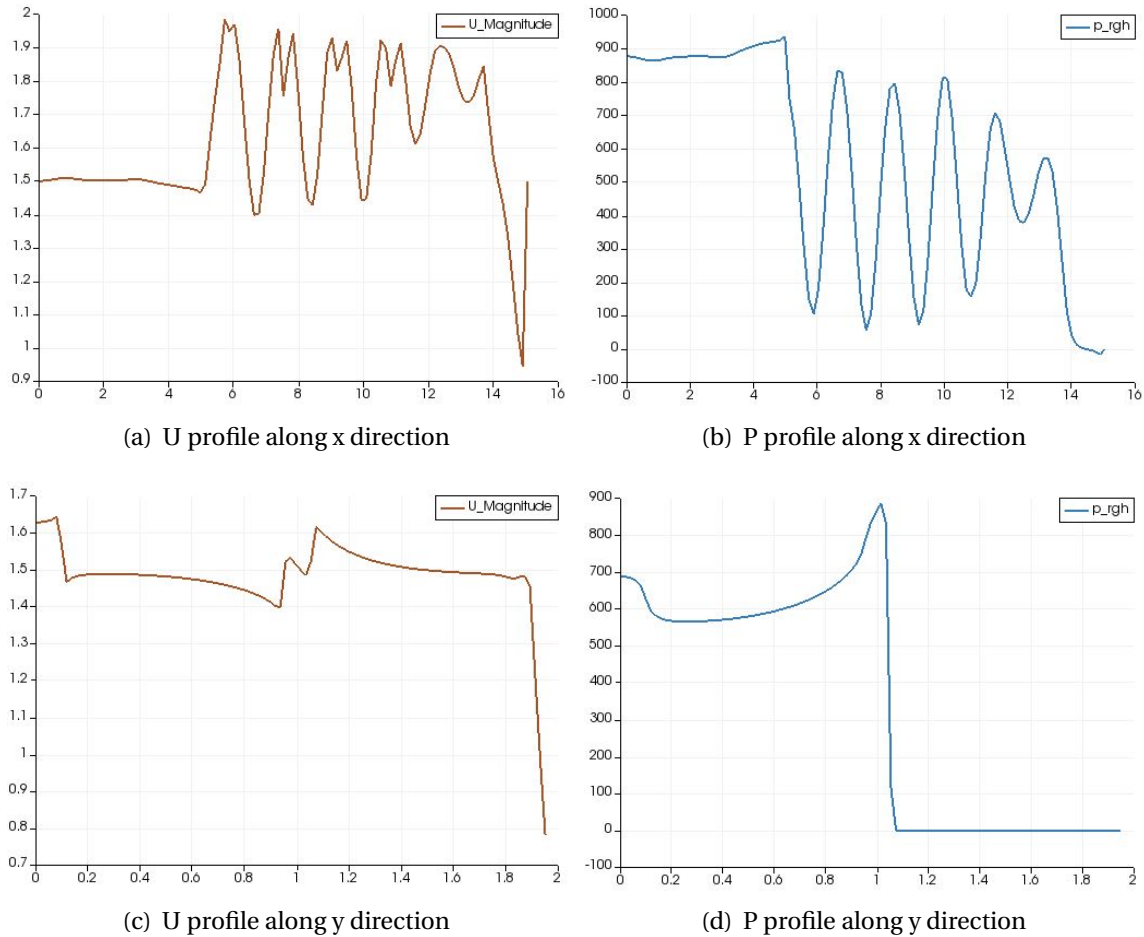


Figure 4.11: Velocity and pressure profile for net with  $Sn=0.217$  at  $U=1.5\text{m/s}$  from side view at the free surface height of the domain along x direction or just behind the porous medium along y direction. horizontal axis: x position from inlet to outlet or y position from bottom to top; vertical axis: velocity or pressure value. (a) U profile along x direction. (b) P profile along x direction. (c) U profile along y direction. (d) P profile along y direction.

Figure 4.12 presents the numerical simulation results of drag force for nets with three different solidity ratios, of which the porous resistance coefficient is derived from the screen force model both in top view case and side view case, as well as the modified Morison model in top view case. The theoretical prediction by screen type force model which has already been used in chapter 3 is also presented here as a standard line. Figure 4.13 presents the numerical simulation results, of which the porous resistance coefficient is derived from the experimental forces. There are results both from top view and side view. The numerical simulation shows a relatively good agreement with the theoretical prediction and the test results respectively. The results with co-

efficient from screen force model in side view case is much closer to the theoretical prediction than the results in top view case. It has the same situation in figure 4.13. From figures one can have an intuitive impression that the results in side view is raised a lot from those in top view. This means, to an extent, the side view case (porous media in free surface condition) is more realistic to model the net panel towing test.

Figure 4.14 and Figure 4.15 shows the numerical simulation results of the corresponding drag coefficients for nets with three different solidity ratios. In figure 4.14, the porous coefficient is derived from the screen force model, which gives an increasing trend with the Reynolds number while in figure 4.15 it gives a descend, in which the porous coefficient is from experimental forces. If one looks at figure 4.16, the drag coefficient for a smooth circular cylinder as function of Reynolds number, in a range of Reynolds number from 2000, the drag coefficient should have an increasing trend since the drag coefficient of screen type force model is deduced from the drag coefficient of circular cylinder. However, the descend in drag coefficient of which porous coefficient is derived from experimental forces tells that the circular cylinder assumption may be not 100% appropriate.

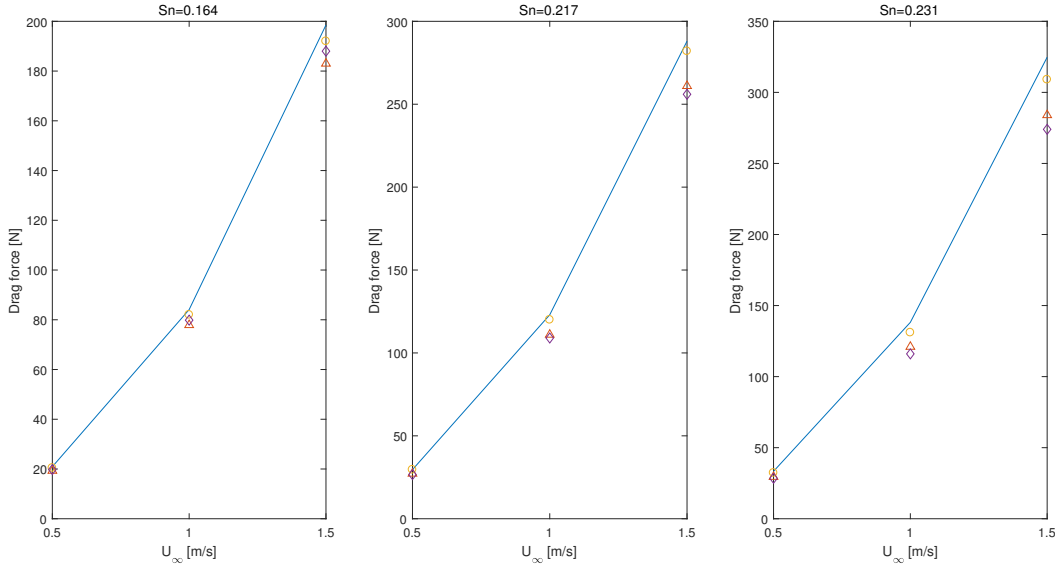


Figure 4.12: Numerical simulation comparison of nets with three different solidity ratios. Blue line: theoretical prediction. The triangles are the results with coefficient from screen force model in top view case; The circles are those in side view case; The diamonds are the results with coefficient from modified Morison model.  $U_\infty$ =incoming flow velocity.

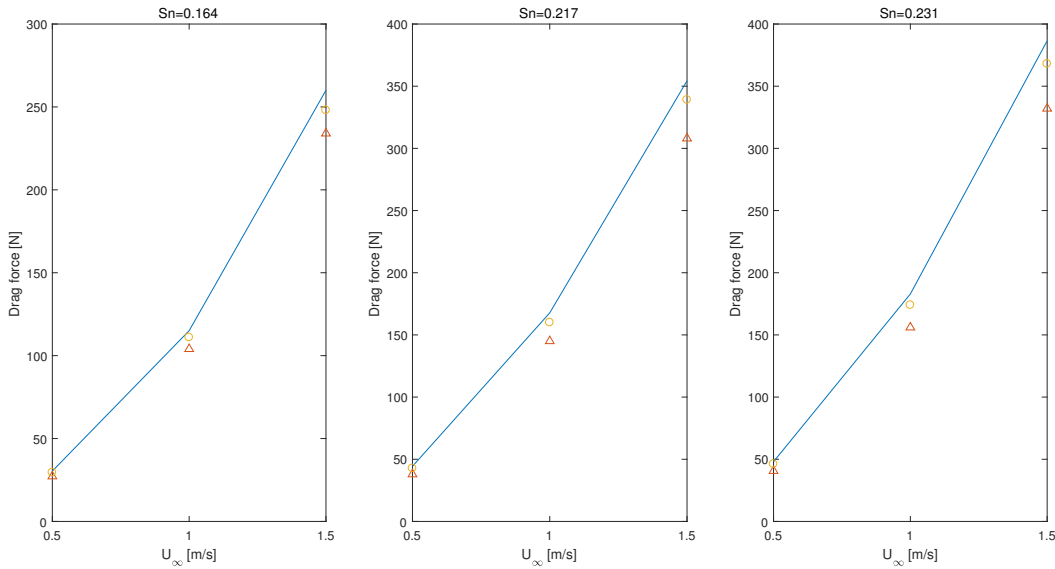


Figure 4.13: Numerical simulation comparison of drag forces for nets with three different solidity ratios. Blue line: test results. The circles are the results with coefficient from the test results in top view case; The triangles are those in side view case.  $U_\infty$ =incoming flow velocity.

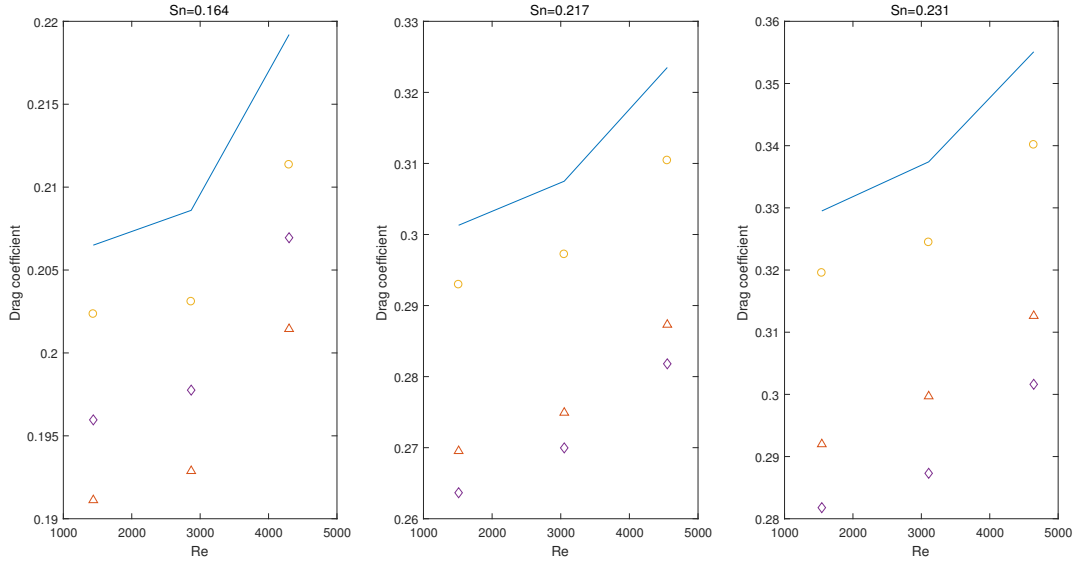


Figure 4.14: Numerical simulation comparison of drag coefficients for nets with three different solidity ratios. Blue line: theoretical prediction. The triangles are the results with coefficient from screen force model in top view case; The circles are those in side view case; The diamonds are the results with coefficient from modified Morison model.  $U_{\infty}$ =incoming flow velocity.

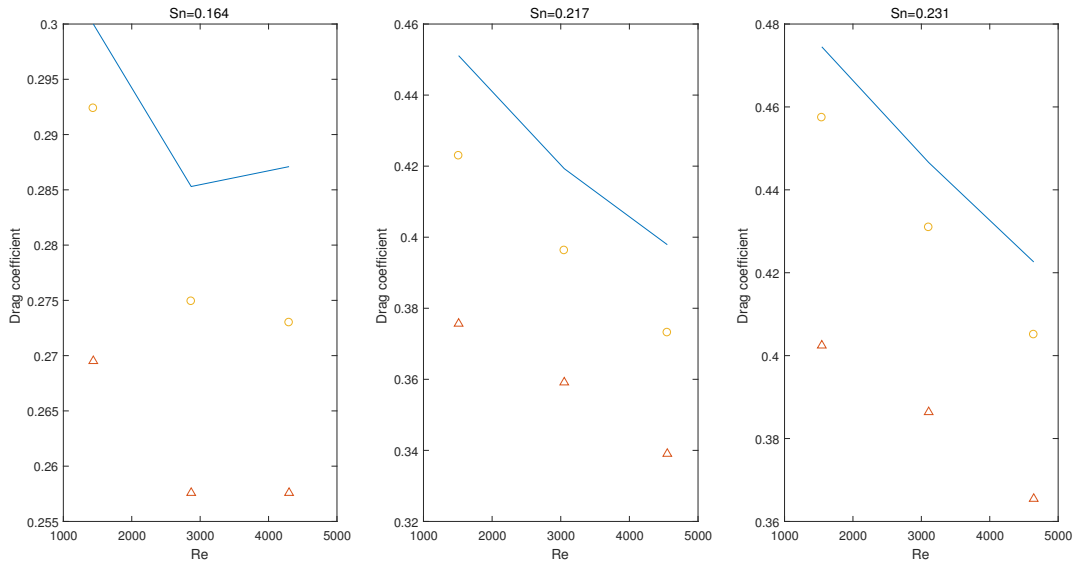


Figure 4.15: Numerical simulation comparison of drag coefficients for nets with three different solidity ratios. Blue line: test results. The circles are the results with coefficient from the test results in top view case; The triangles are those in side view case.  $U_{\infty}$ =incoming flow velocity.

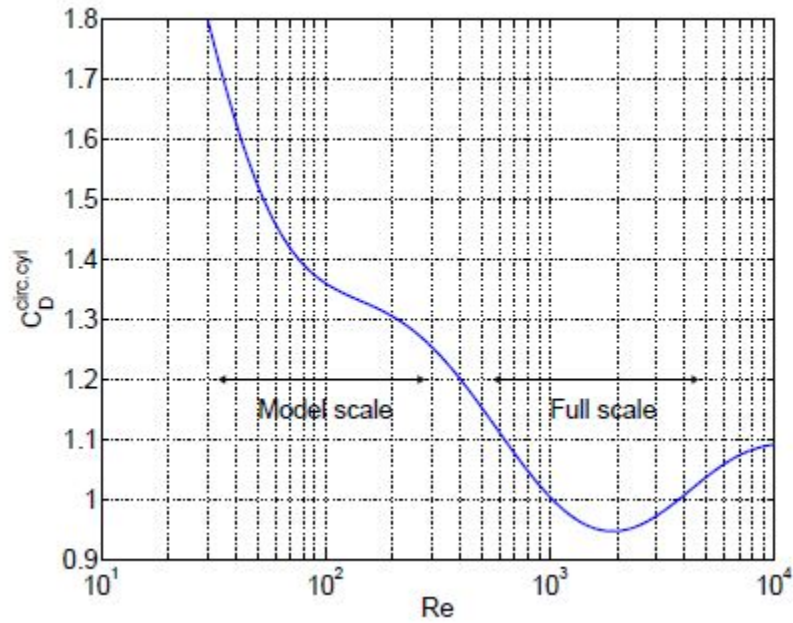


Figure 4.16: The drag coefficient for a smooth circular cylinder as function of Reynolds's number, given as a 7th order polynomial from curvefitting data in the literature. (Kristiansen (2013))

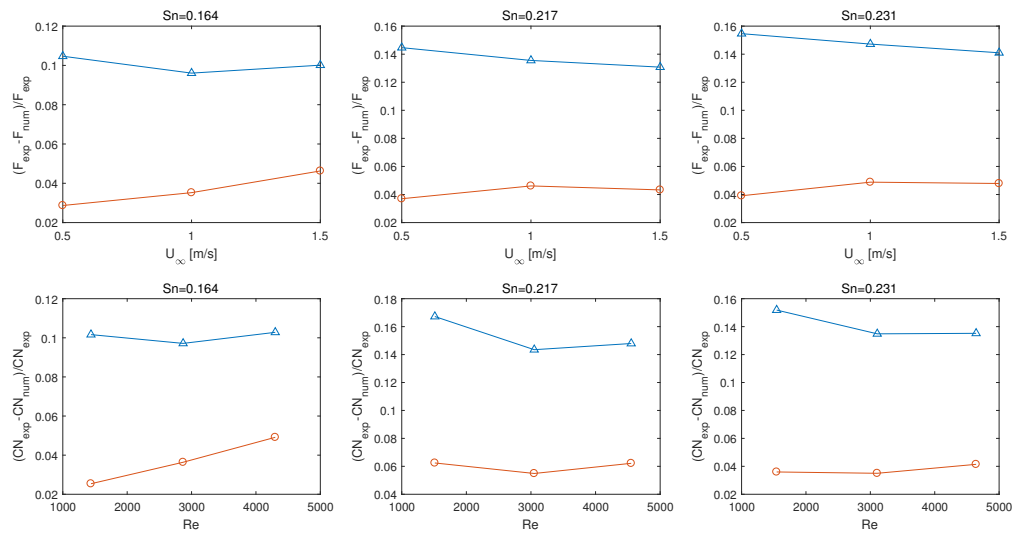


Figure 4.17: The relative error between numerical results and experimental results, of which the porous resistance coefficient is derived from test results. Blue line with triangle: relative error between experimental results and numerical results from top view. Red line with circle: relative error between experimental results and numerical results from side view.

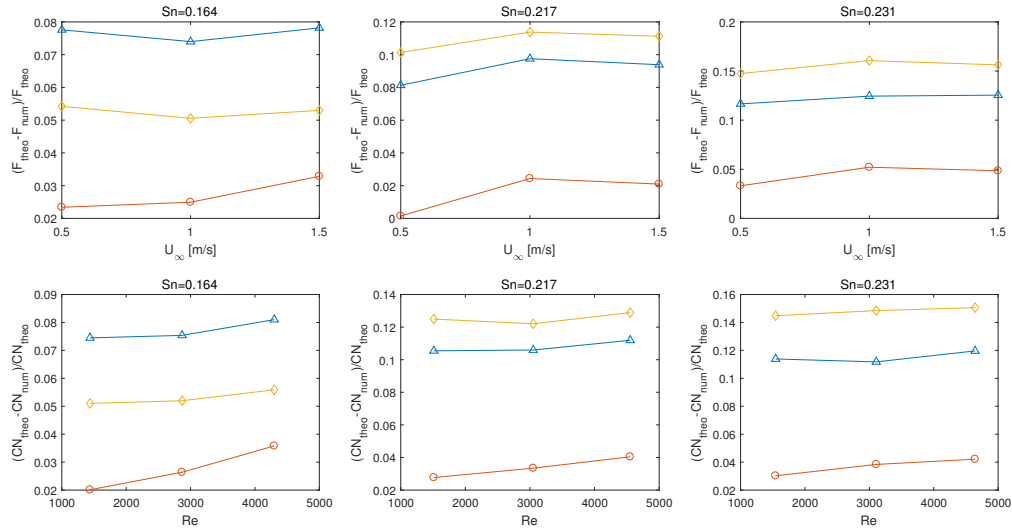


Figure 4.18: The relative error between numerical results and theoretical results, of which the porous resistance coefficient is derived from force models. Blue line with triangle: relative error between theoretical results and numerical results (Screen type force model) from top view. Red line with circle: relative error between theoretical results and numerical results (Screen type force model) from side view. Yellow line with diamond: relative error between theoretical results and numerical results (modified Morison model) from top view.

Figure 4.17 and Figure 4.18 give the relative error between forces and force coefficients corresponding to figure 4.12 to 4.17. For side view cases, the relative errors are almost all below 5%, which turns to be a good prediction. Relative errors from all cases, for both forces and force coefficients are under 18%.

### 4.3 Comments

The porous media model is a good proposal for modelling the net panel. The free surface elevation in the towing tank can be modelled well with a two-phase flow porous media model. Hexahedral mesh is applied in CFD simulation. The mesh scheme applied in this thesis is limited to the time and computer source. A finer mesh scheme could be expected.

The porous media in a two-phase flow (side view) gives a better fit than it in the single phase flow (top view) no matter for the force model porous coefficient or experimental force porous

coefficient. It also reflects the force oscillation which is a more realistic case.

However, the numerical model is in 2D case, which means the flow variation in z direction is forced to be zero, leading to no force contribution from z direction. The drag force may thus be under-predicted in numerical simulation. 3D model has to be built in the future work to verify if it gives better results.

# Chapter 5

## Conclusion

A series of net panel towing tests has been carried out. Resistance force on the net panel was measured. The nets have been tested in current only condition, wave only condition and current with wave condition with a representative range of current velocity, wave period and wave steepness. Numerical simulations were implemented. Porous media model has been applied to represent the net panel in the towing tank. The net was modelled as a porous medium both in a single phase flow condition and two-phase flow condition. The porous resistance was expressed by D'arcy and Forchheimer equation, in which the quadratic porous coefficient was derived from both experimental force and rational force models. The porous resistance force was obtained from numerical simulation to compare with the drag force in current only condition from experiments. Satisfactory agreement between simulations and experiments was demonstrated.

There were errors and uncertainties in the experiments. The limitation of the towing tank environment lead to a careful study on the error bound of the experimental results. One of the main uncertainty lies in estimating the solidity ratio. The frame which the net was stretched onto has a large effect on the resistance force of the net panel.

The porous media is a good proposal for modelling the net panel. The free surface elevation in the towing tank can be modelled well with a two-phase flow porous media model. The porous media in a two-phase flow (side view) turns to give a better agreement.

## 5.1 Further Work

- The frame has a large effect on the resistance force of the net panel. An improvement is expected for frame which has a more streamlined body and smaller effect on the net.
- Force on HDPE nets give more uncertainties when using the screen type force model to predict the drag force on the net. Therefore, an improved force model could be studied, i.e.  $F_D = F_D^{cir.cyl} + F_D^{knot}$ , where  $F_D^{knot}$  can be modelled as the drag force on a sphere.
- The free surface can to some extent affect the drag force on net panel in current only condition. Thus, tests with net panel in a flume (meaning that there is no free surface) are expected to realize in the future.
- Wave generation in the towing tank is not idealistic due to the equipment limitation. So a further study on wave force on net panel is desired.
- Net combined with frame is expected to realize in CFD simulation to make more physical simulation of flow through and around the net panel.
- Wave is expected to be implemented in the CFD simulation and a 3D model is to be built.

# Appendix A

## Sn results by GIMP

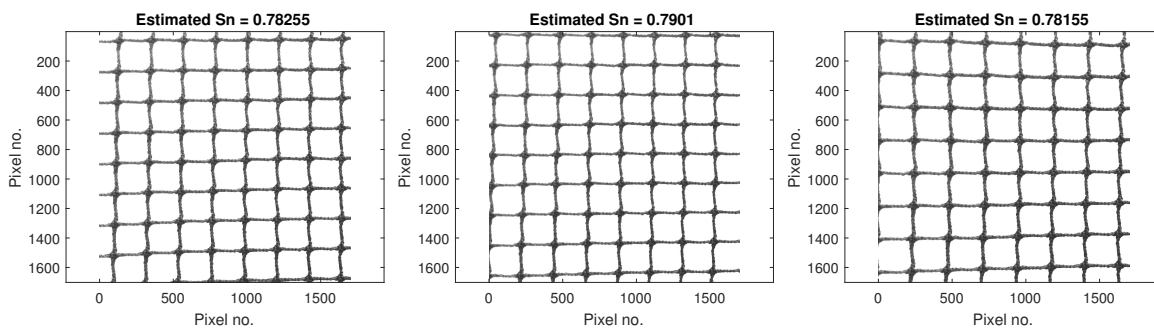


Figure A.1: Comparison of estimated solidity ratios by GIMP for the same net. The net has a final solidity ratio value of  $S_n = 0.217$ .

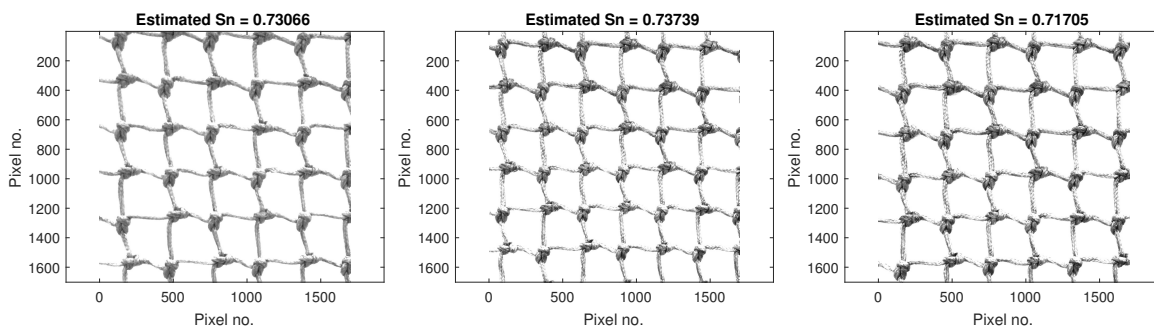


Figure A.2: Comparison of estimated solidity ratios by GIMP for the same net. The net has a final solidity ratio value of  $S_n = 0.27$ .

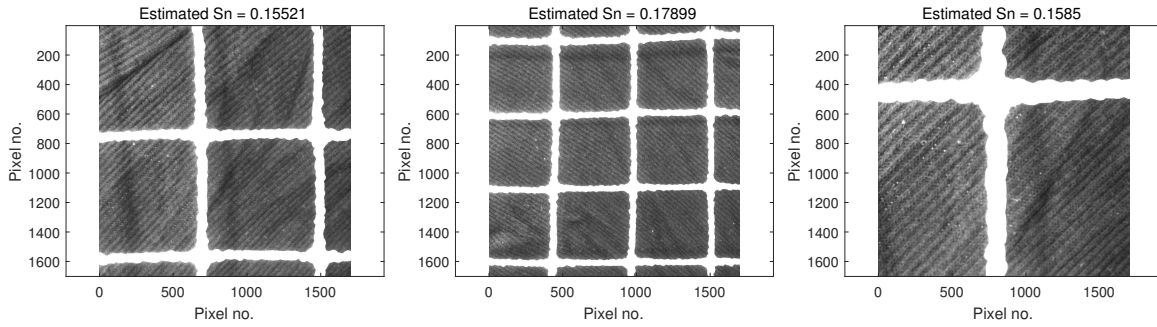


Figure A.3: Comparison of estimated solidity ratios by GIMP for the same net. The net has a final solidity ratio value of  $S_n = 0.164$ .

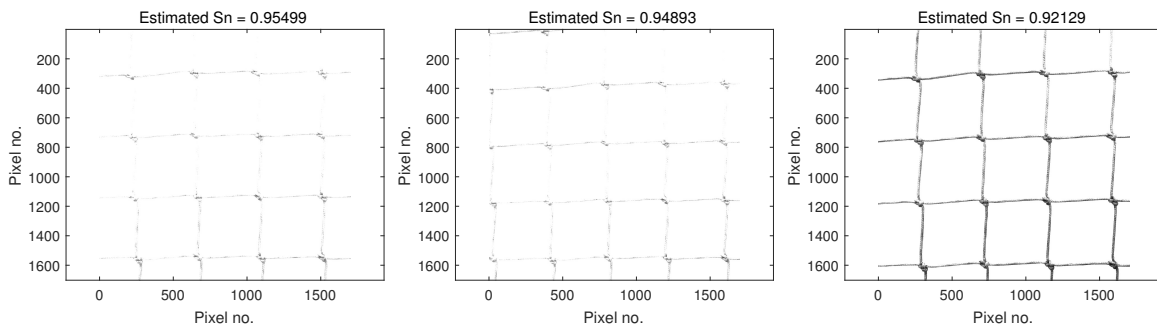


Figure A.4: Comparison of estimated solidity ratios by GIMP for the same net. The net has a final solidity ratio value of  $S_n = 0.079$ .

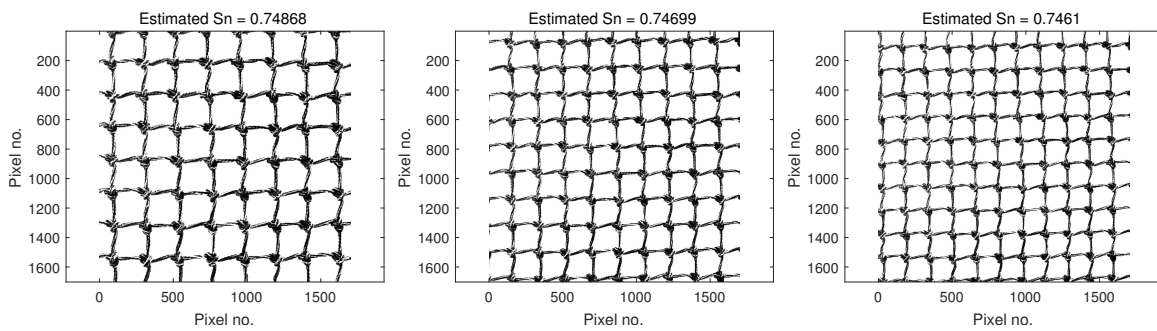


Figure A.5: Comparison of estimated solidity ratios by GIMP for the same net. The net has a final solidity ratio value of  $S_n = 0.253$ .

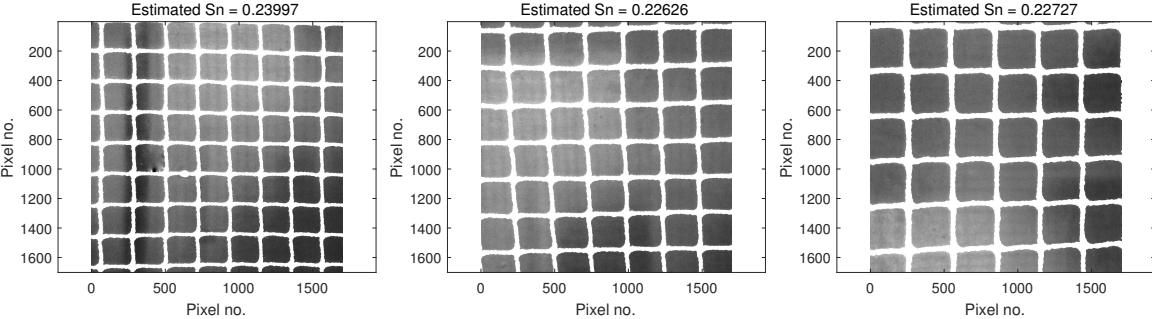


Figure A.6: Comparison of estimated solidity ratios by GIMP for the same net. The net has a final solidity ratio value of  $S_n = 0.231$ .

# Appendix B

## Power Spectral Density

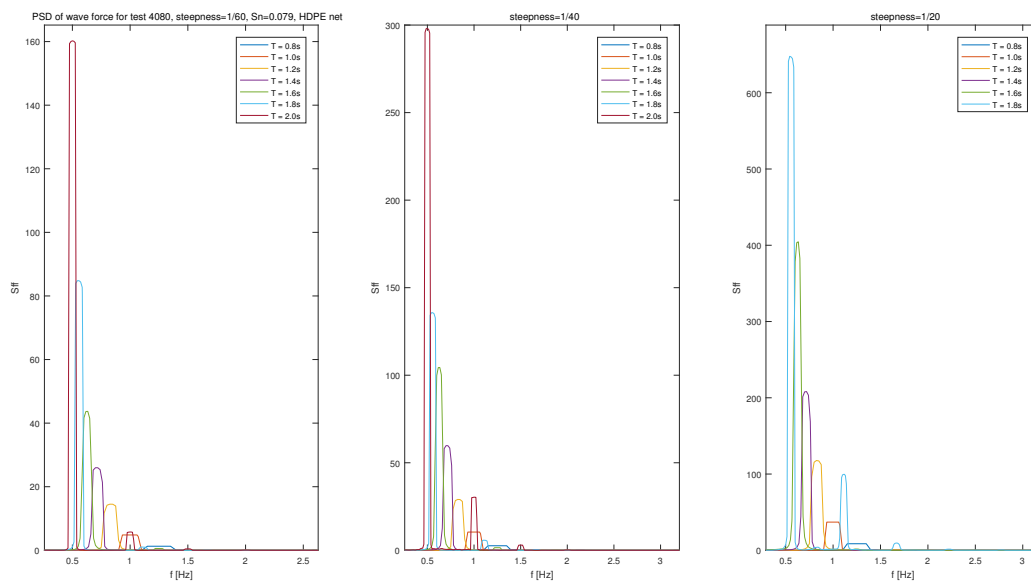


Figure B.1: Power spectral density of wave force for test 4080, HDPE net with Sn=0.079

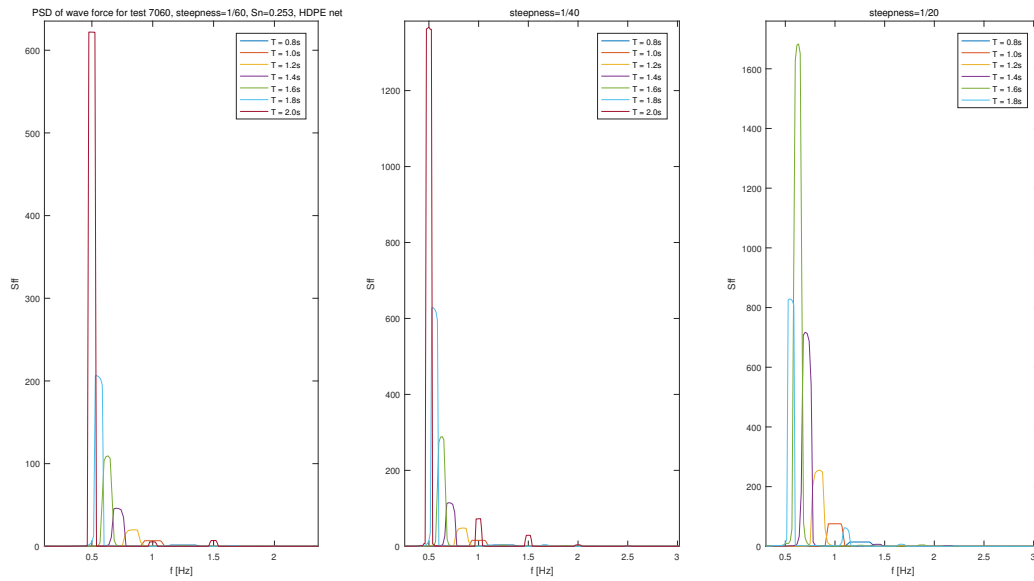


Figure B.2: Power spectral density of wave force for test 7060, HDPE net with Sn=0.253

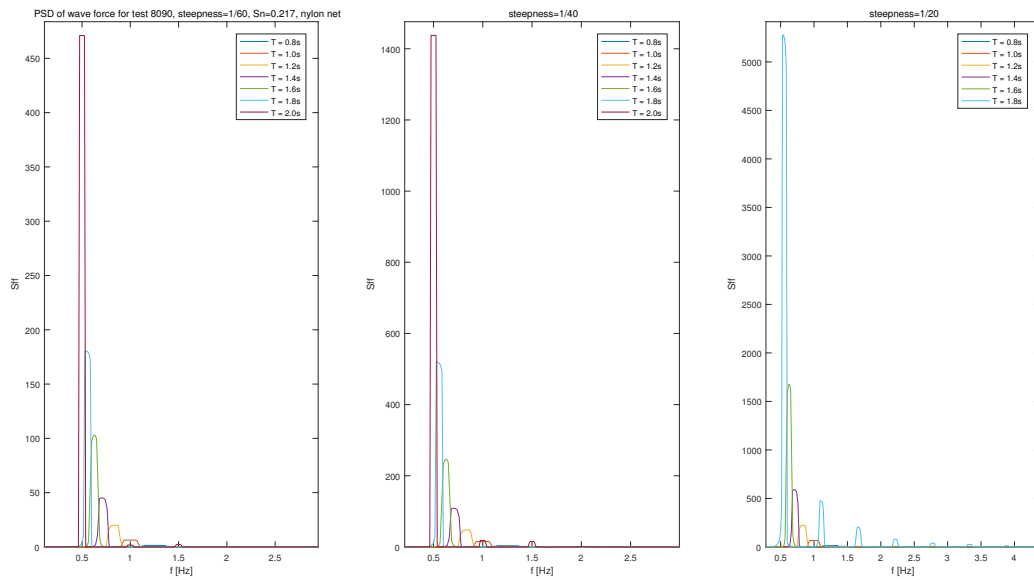


Figure B.3: Power spectral density of wave force for test 8090, nylon net with Sn=0.217

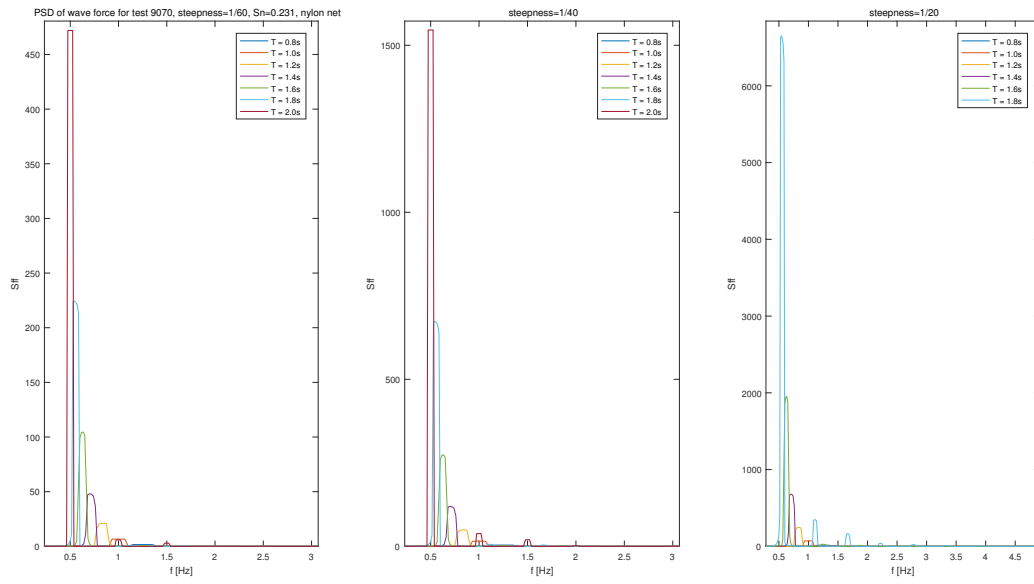


Figure B.4: Power spectral density of wave force for test 9070, nylon net with Sn=0.231

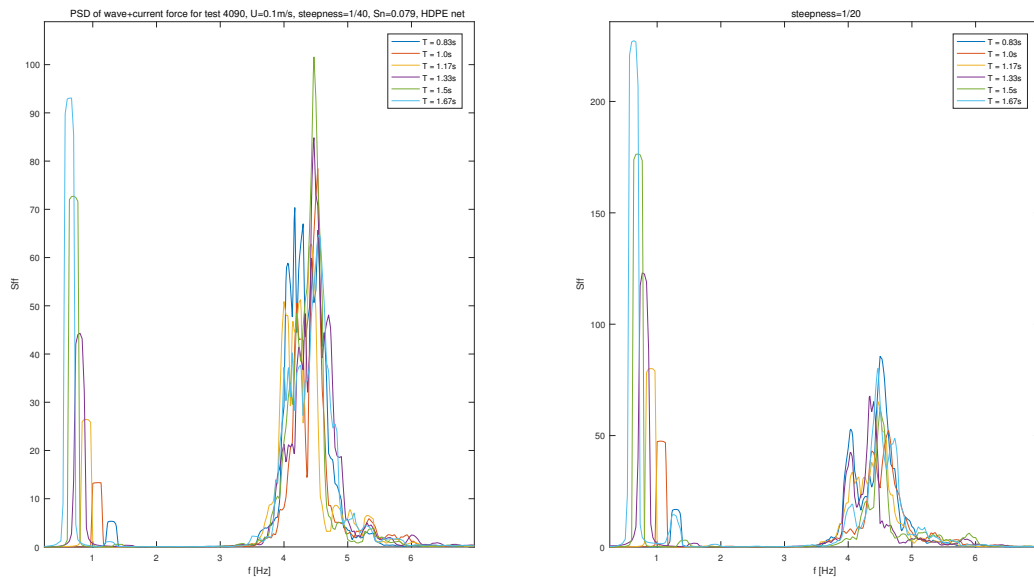


Figure B.5: Power spectral density of wave force for test 4090, HDPE net with Sn=0.079, u=0.1m/s

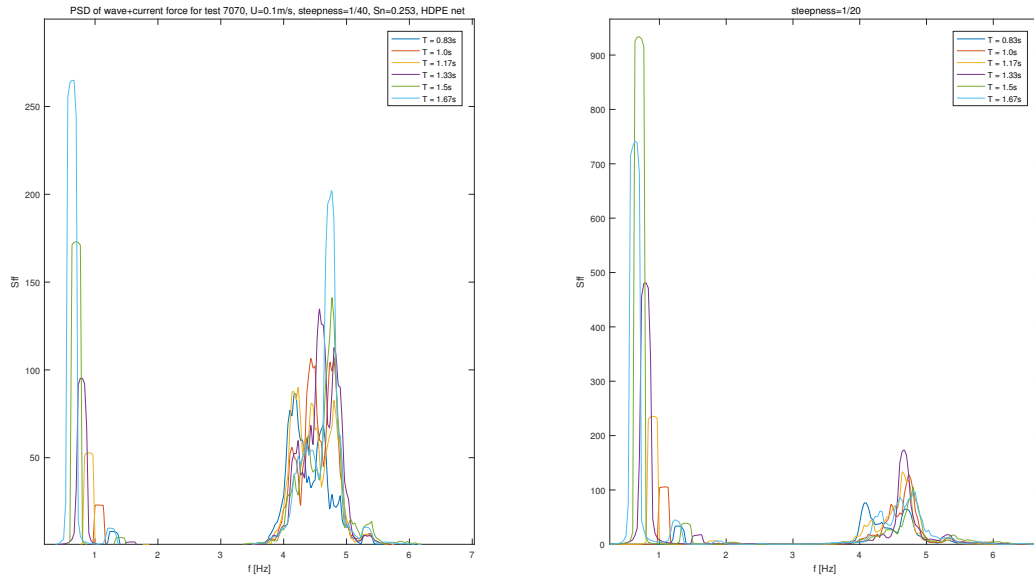


Figure B.6: Power spectral density of wave+current force for test 7070, HDPE net with  $S_n=0.253$ ,  $u=0.1\text{m/s}$

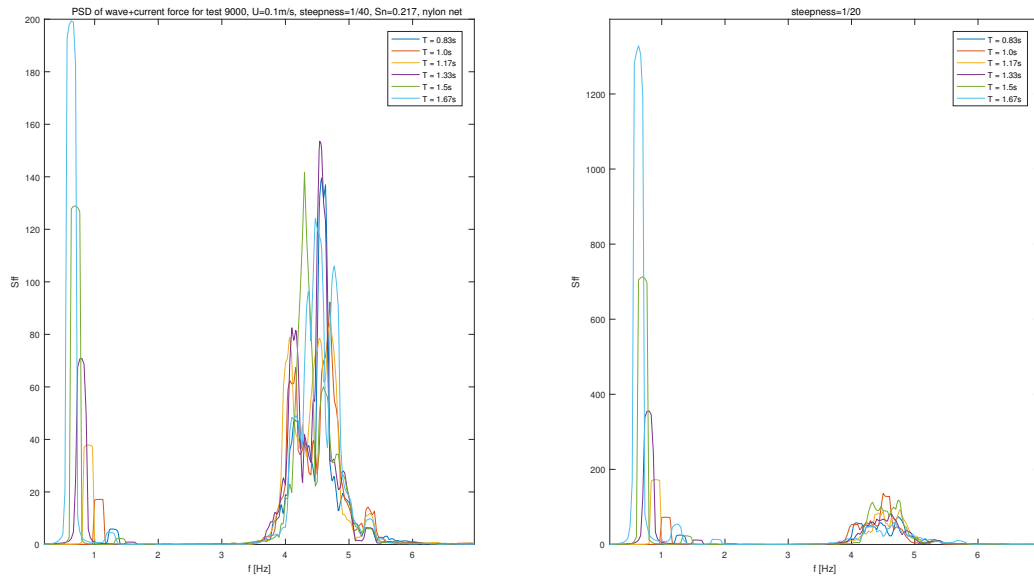


Figure B.7: Power spectral density of wave+current force for test 9000, nylon net with  $S_n=0.217$ ,  $u=0.1\text{m/s}$

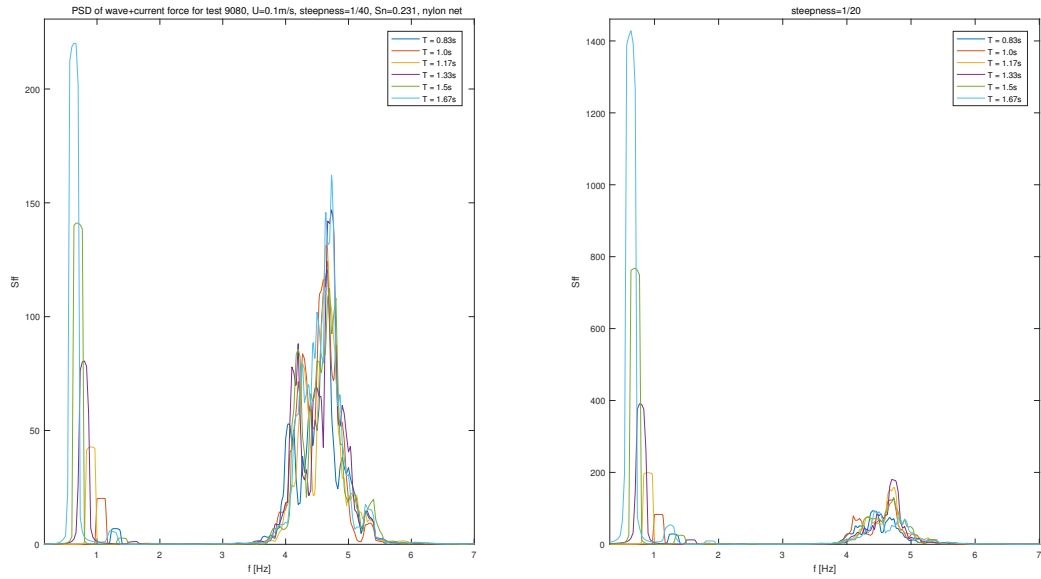


Figure B.8: Power spectral density of wave+current force for test 9080, nylon net with  $S_n=0.231$ ,  $u=0.1\text{m/s}$

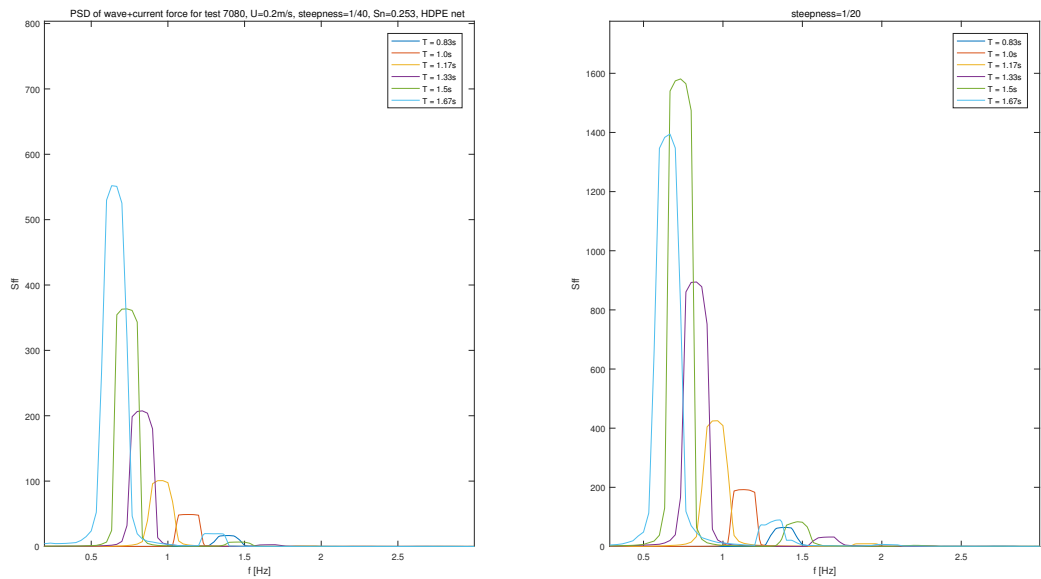


Figure B.9: Power spectral density of wave+current force for test 7080, HDPE net with  $S_n=0.253$ ,  $u=0.2\text{m/s}$

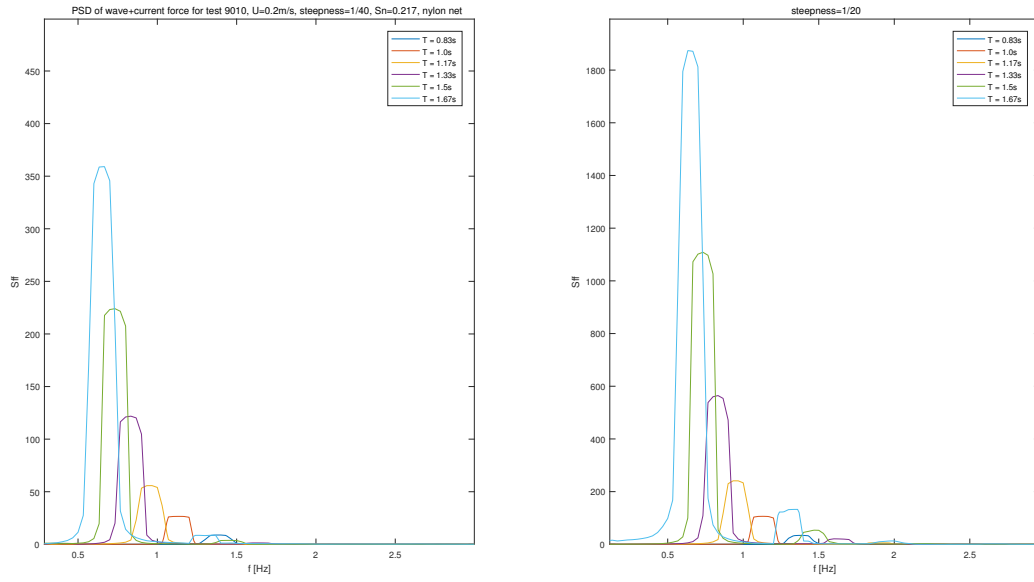


Figure B.10: Power spectral density of wave+current force for test 9010, nylon net with  $S_n=0.217$ ,  $u=0.2\text{m/s}$

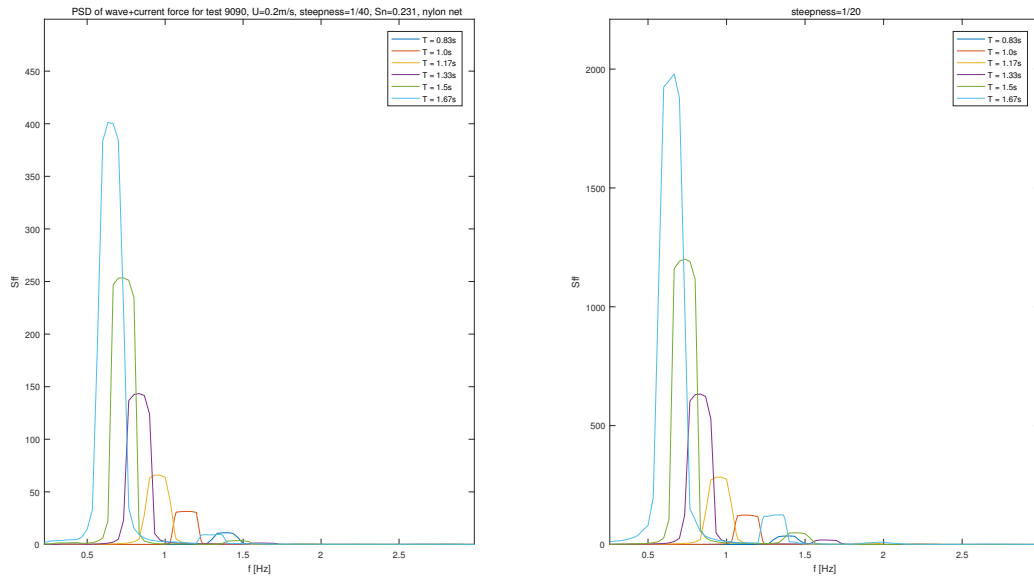


Figure B.11: Power spectral density of wave+current force for test 9090, nylon net with  $S_n=0.231$ ,  $u=0.2\text{m/s}$

# Appendix C

## Time Series

### C.1 Current Only

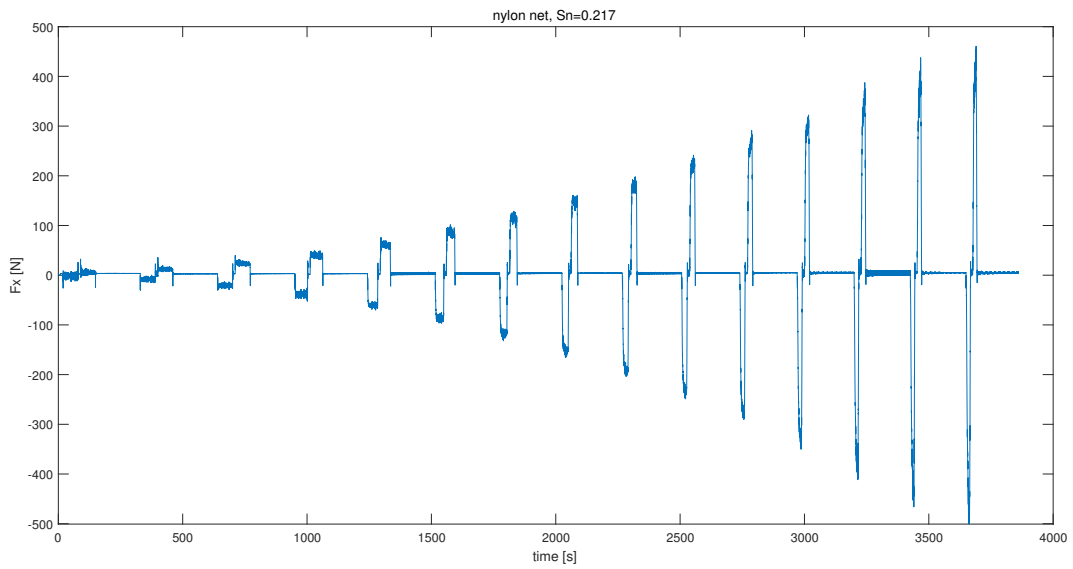


Figure C.1: Time series of Drag force in current only condition

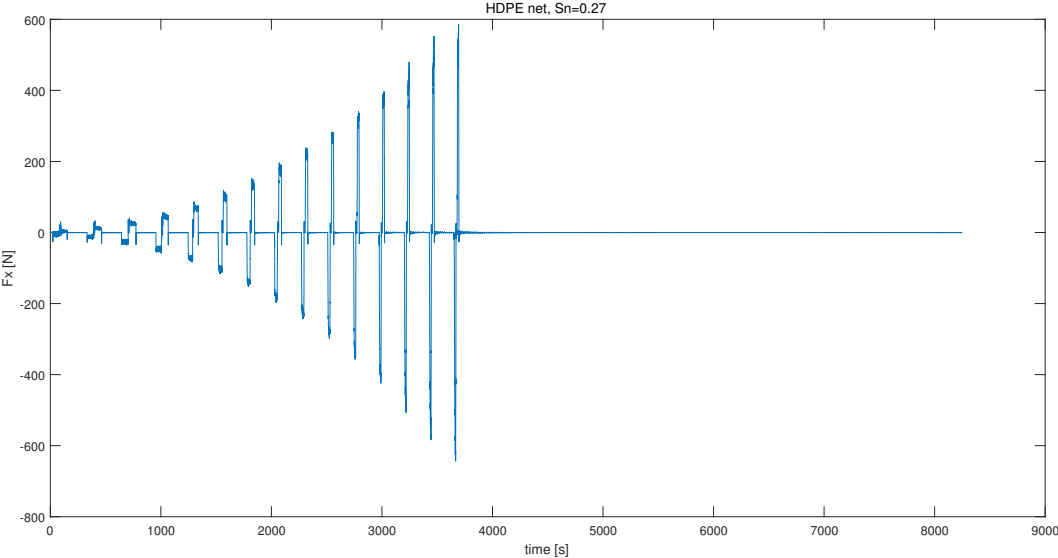


Figure C.2: Time series of Drag force in current only condition

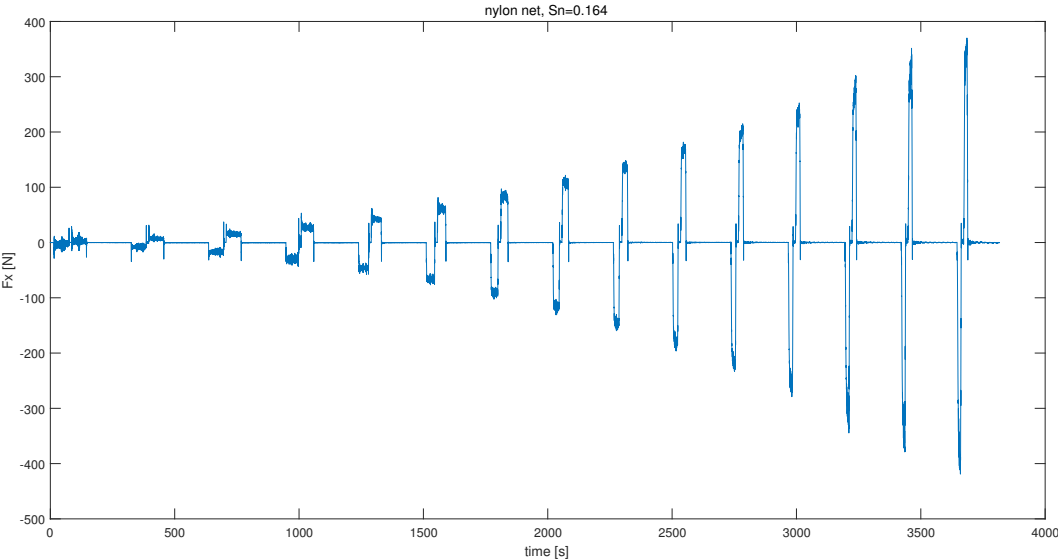


Figure C.3: Time series of Drag force in current only condition

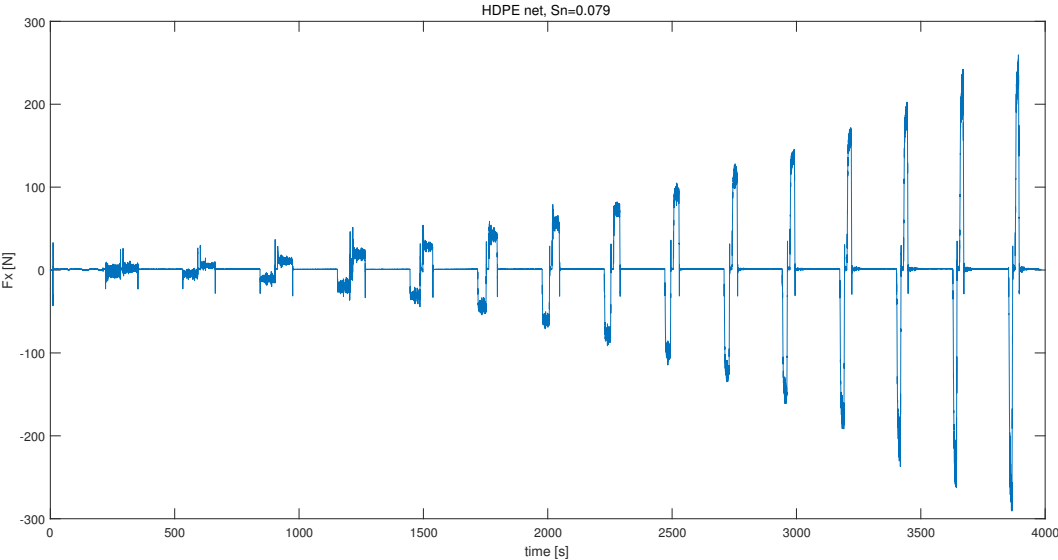


Figure C.4: Time series of Drag force in current only condition

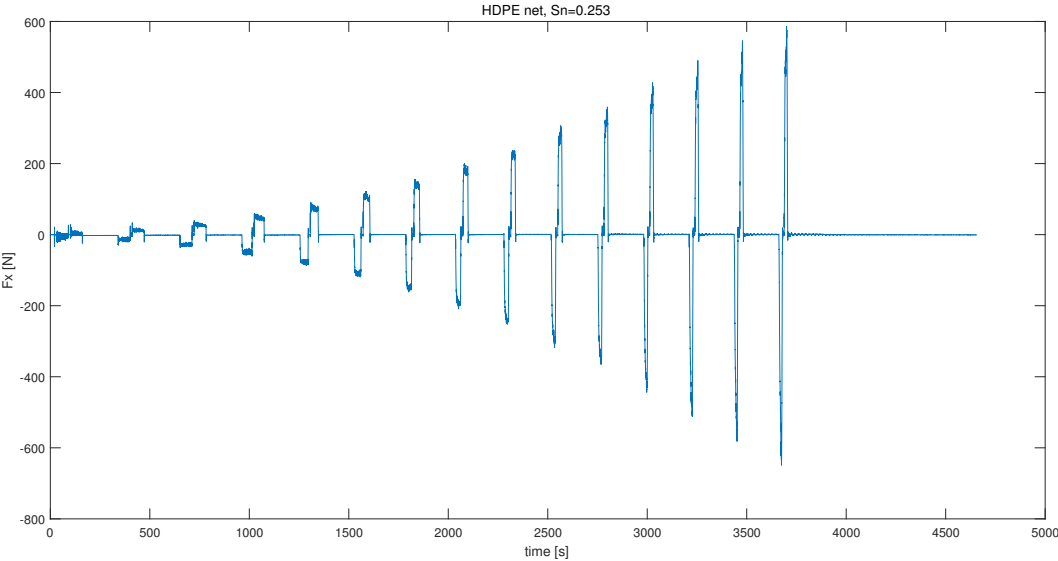


Figure C.5: Time series of Drag force in current only condition

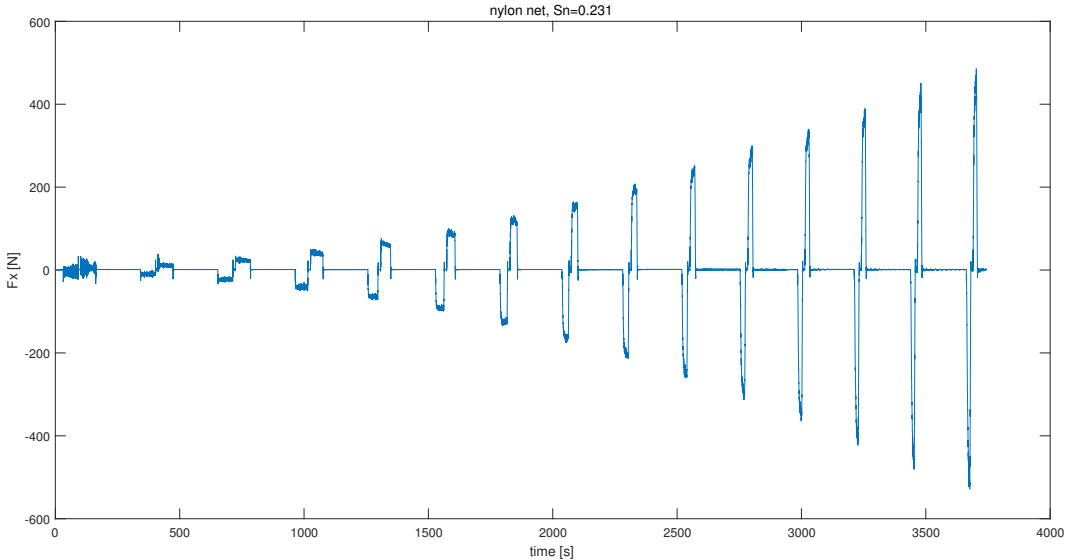


Figure C.6: Time series of Drag force in current only condition

### C.2 Wave Only

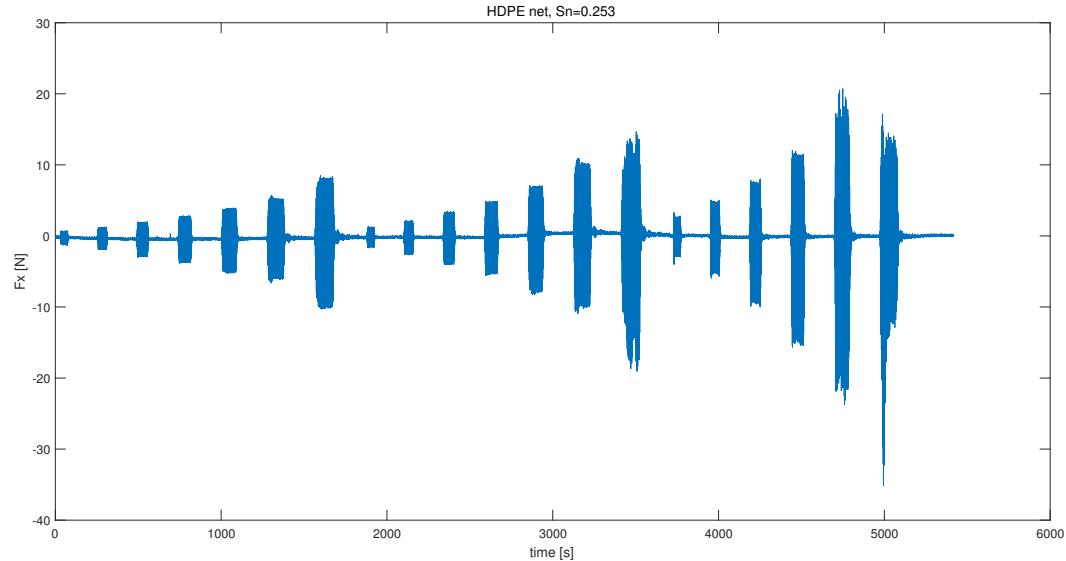


Figure C.7: Time series of Drag force in wave only condition

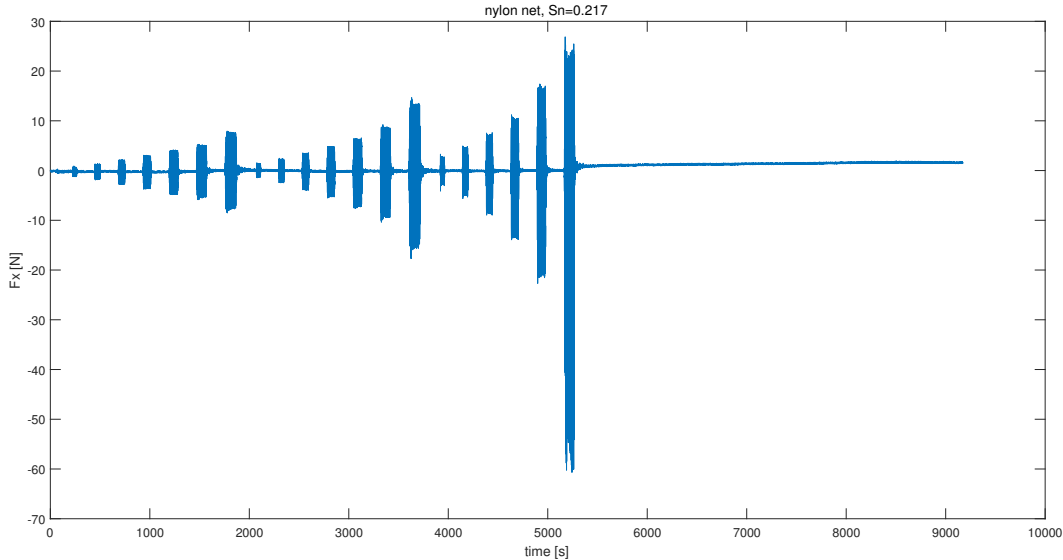


Figure C.8: Time series of Drag force in wave only condition

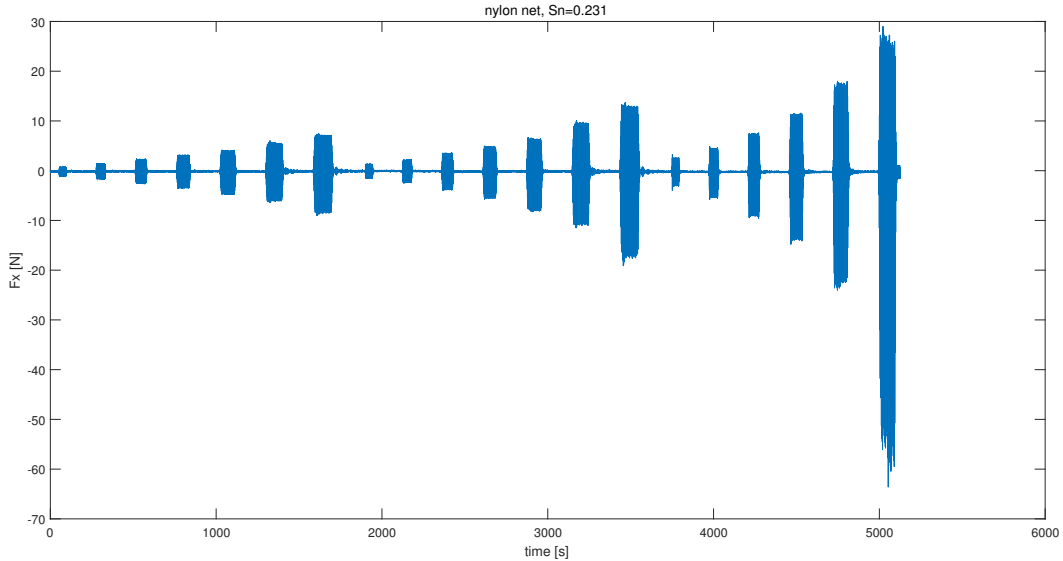


Figure C.9: Time series of Drag force in wave only condition

### C.3 Current with Wave

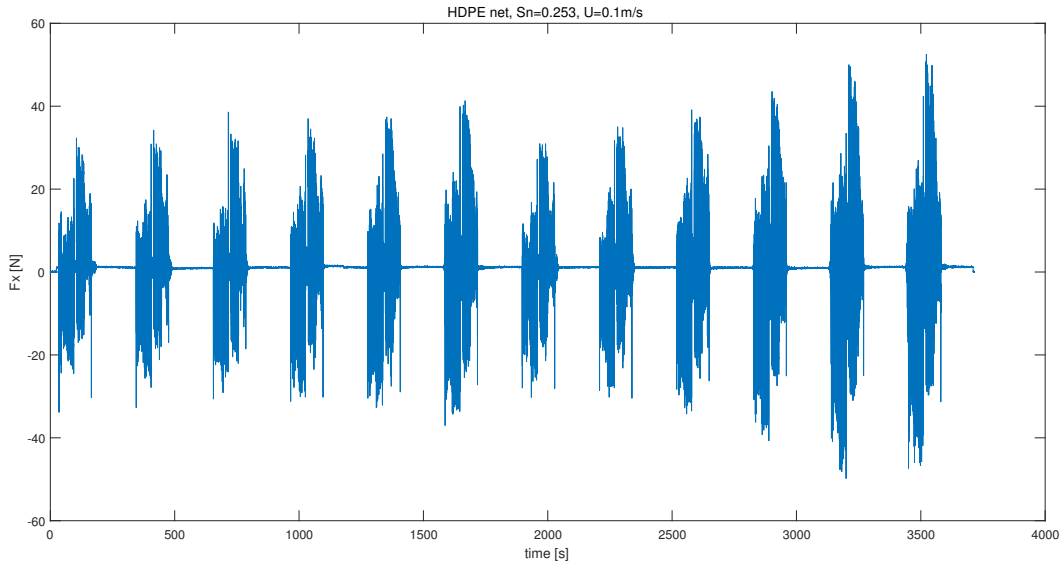


Figure C.10: Time series of Drag force in current and wave condition

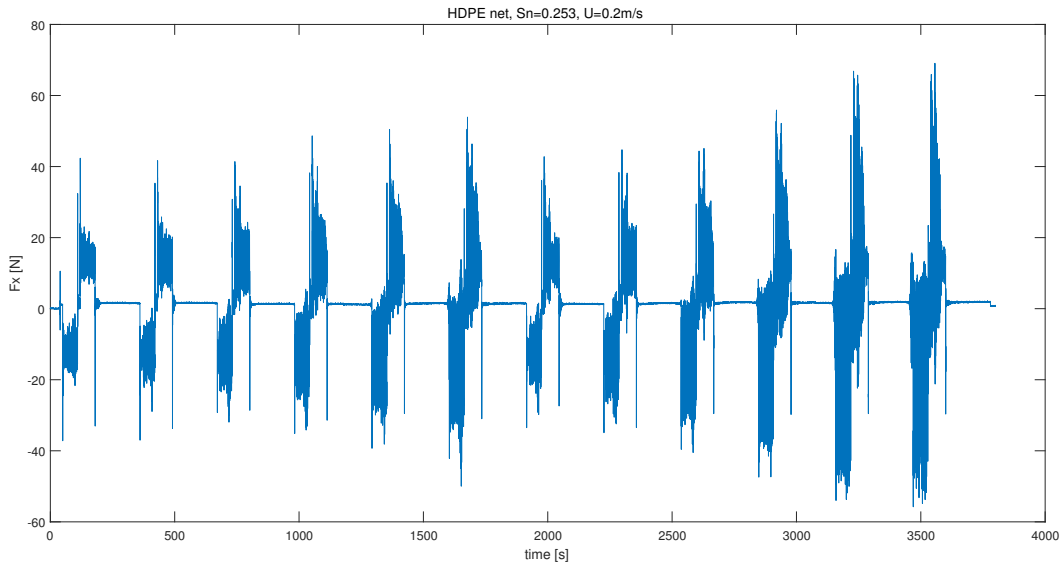


Figure C.11: Time series of Drag force in current and wave condition

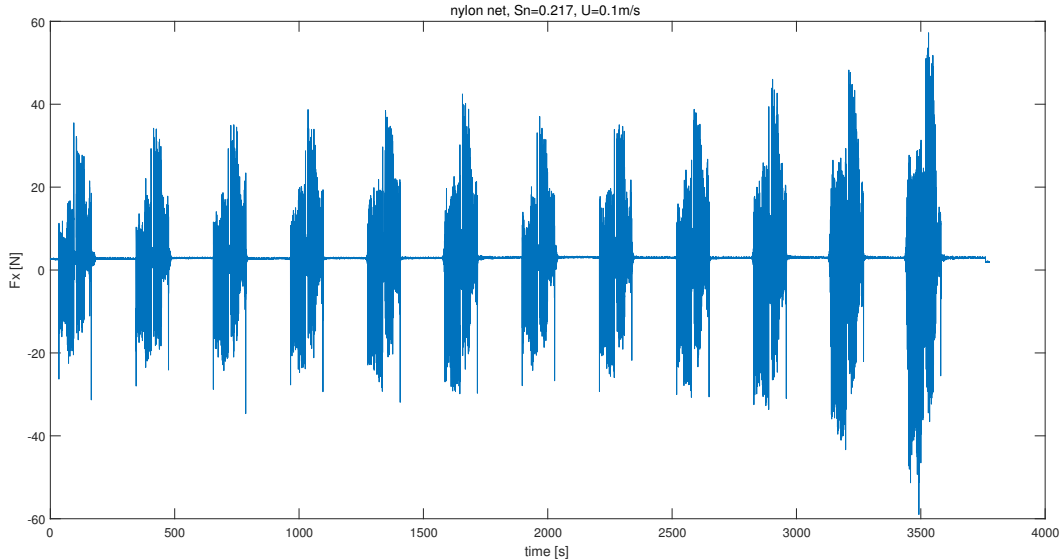


Figure C.12: Time series of Drag force in current and wave condition

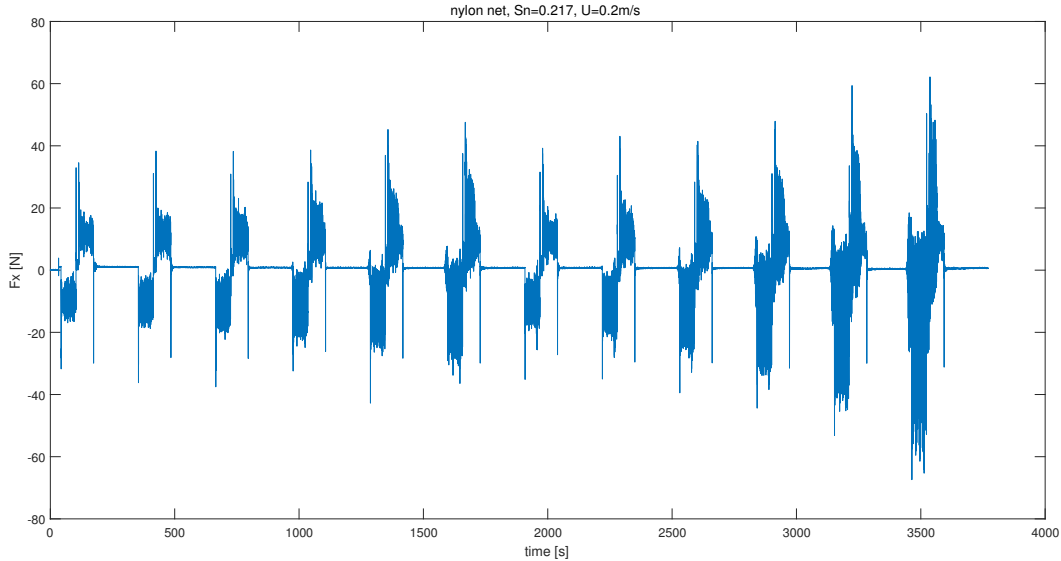


Figure C.13: Time series of Drag force in current and wave condition

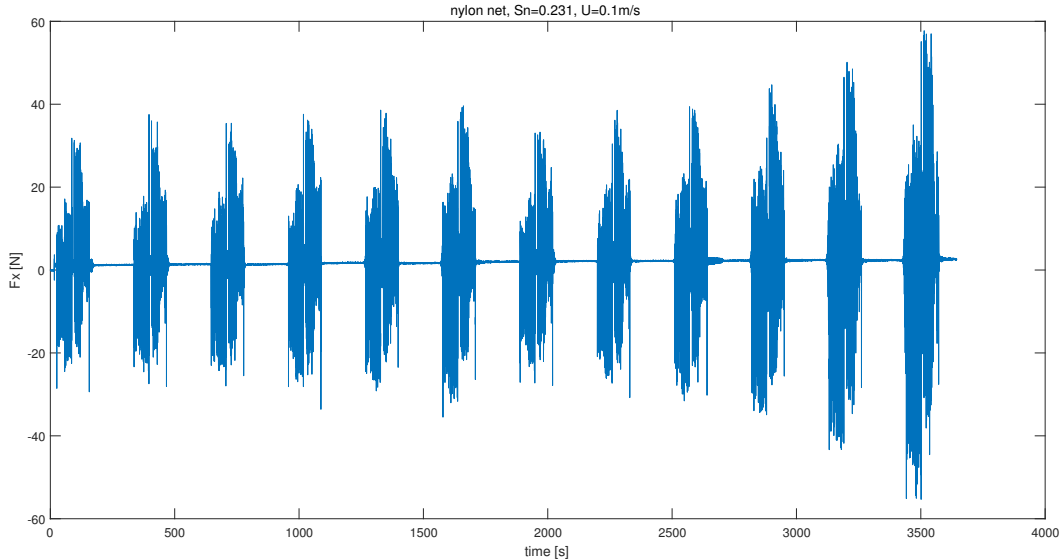


Figure C.14: Time series of Drag force in current and wave condition

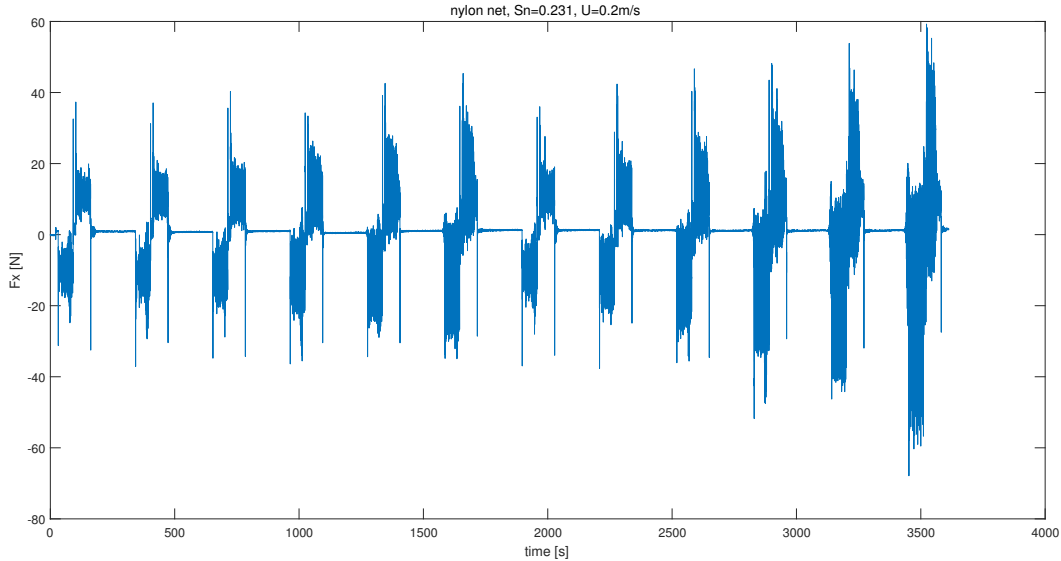


Figure C.15: Time series of Drag force in current and wave condition

# Bibliography

- Bi, C.-W., Zhao, Y.-P., Dong, G.-H., Zheng, Y.-N., and Gui, F.-K. (2014). A numerical analysis on the hydrodynamic characteristics of net cages using coupled fluid–structure interaction model. *Aquacultural Engineering*, 59:1–12.
- Blevins, R. D. (1984). *Applied fluid dynamics handbook*, volume 1.
- Chen, H. and Christensen, E. D. (2016). Investigations on the porous resistance coefficients for fishing net structures. *Journal of Fluids and Structures*, 65:76–107.
- Goldstein, S. (1938). *Modern developments in fluid dynamics: an account of theory and experiment relating to boundary layers, turbulent motion and wakes*, volume 1. Clarendon Press.
- Greenshields, C. J. (2015). *Openfoam user guide*, volume 3.
- Jensen, B., Jacobsen, N. G., and Christensen, E. D. (2014). Investigations on the porous media equations and resistance coefficients for coastal structures. *Coastal Engineering*, 84:56–72.
- Kristiansen, T. (2013). A numerical parameter study on current forces on circular aquaculture net cages. In *ASME 2013 32nd International Conference on Ocean, Offshore and Arctic Engineering*, pages V009T12A035–V009T12A035. American Society of Mechanical Engineers.
- Kristiansen, T. and Faltinsen, O. M. (2012). Modelling of current loads on aquaculture net cages. *Journal of Fluids and Structures*, 34:218–235.
- Kristiansen, T. and Faltinsen, O. M. (2015). Experimental and numerical study of an aquaculture net cage with floater in waves and current. *Journal of Fluids and Structures*, 54:1–26.

- Lader, P. F. and Fredheim, A. (2006). Dynamic properties of a flexible net sheet in waves and current—a numerical approach. *Aquacultural engineering*, 35(3):228–238.
- Patursson, Ø., Swift, M. R., Tsukrov, I., Simonsen, K., Baldwin, K., Fredriksson, D. W., and Cellikol, B. (2010). Development of a porous media model with application to flow through and around a net panel. *Ocean Engineering*, 37(2):314–324.
- Rudi, H., Løland, G., and Furunes, I. (1988). Experiments with nets; forces on and flow trough net panels and cage systems. *MT 51 F88*, 215.
- Zhan, J., Jia, X., Li, Y., Sun, M., Guo, G., and Hu, Y. (2006). Analytical and experimental investigation of drag on nets of fish cages. *Aquacultural engineering*, 35(1):91–101.
- Zhao, Y.-P., Bi, C.-W., Dong, G.-H., Gui, F.-K., Cui, Y., Guan, C.-T., and Xu, T.-J. (2013). Numerical simulation of the flow around fishing plane nets using the porous media model. *Ocean Engineering*, 62:25–37.
- Zhao, Y.-P., Bi, C.-W., Liu, Y.-X., Dong, G.-H., and Gui, F.-K. (2014). Numerical simulation of interaction between waves and net panel using porous media model. *Engineering Applications of Computational Fluid Mechanics*, 8(1):116–126.